TOPOGRAPHY OF CLOSED DEPRESSIONS, SCARPS, AND GRABENS IN THE NORTH THARSIS REGION OF MARS: IMPLICATIONS FOR SHALLOW CRUSTAL DISCONTINUITIES AND GRABEN FORMATION

Philip A. Davis
Kenneth L. Tanaka

U.S. Geological Survey
2255 North Gemini Drive
Flagstaff, Arizona 86001
602-556-7000
fax 602-556-7014
SPAN ASTROG::PDAVIS
INTERNET: PDAVIS@ASTROG.SPAN.NASA.GOV

Matthew P. Golombek

Jet Propulsion Laboratory
4800 Oak Grove Drive
Pasadena, California 91109
818-354-3883
fax 818-393-1227

43 Manuscript pages
14 Figures
3 Tables

Key Words: Geological Processes, Mars; Mars, surface; Tectonics

Submitted Feb. 22, 1994 to Icarus
Revised Nov. 14, 1994

Running Title: Landform morphometries in the north Tharsis region, Mars

Correspondence: Philip Davis
Branch of Astrogeology
U.S. Geological Survey
2255 North Gemini Drive
Flagstaff, AZ 86001

ABSTRACT

Using Viking Orbiter images, detailed photoclinometric profiles were obtained across 10 irregular depressions, 32 fretted fractures, 49 troughs and pits, 124 solitary scarps, and 370 simple grabens in the north Tharsis region of Mars. These data allow inferences to be made on the shallow crustal structure of this region. "he frequency modes of measured scarp heights correspond with previous general thickness estimates of the heavily cratered and ridged plains units. The depths of the fiat-floored irregular depressions (55-175 m), fretted fractures (85-890 m), and troughs and pits (60- 1,620 m) are also similar to scarp heights (thicknesses) of the geologic units in which these depressions occur, which suggests that the depths of these flat-floored features were controlled by erosional base levels created by lithologic contacts. Although the features have a similar age, both their depths and their observed local structural control increase in the order l i steal above, which suggests that the more advanced stages of associated fracturing facilitated the development of these depressions by increasing permeability. If a ground-ice zone is a factor in development of these features, as has been suggested, our observation that the depths of these features decrease with increasing latitude suggests that either the thickness of the ground-ice zone does not increase poleward or the depths of the depressions were. controlled by the top of the ground-ice zone whose depth may decrease with latitude.

Deeper discontinuities are inferred from fault-intersection depths of 370 simple grabens (assuming 60° dipping faults that initiate at a mechanical discontinuity) in Tempe Terra and Alba Patera and from the depths of the large, flat-floored troughs in Tempe Terra. The frequency distributions of these fault-intersection and large trough depths show a

concentration at 1.0- 1.6 km depth, similar to data obtained for Syria, Sinai, and Lunae Plana. The consistency of these depth data over such a large region of western Mars suggests that a discontinuity or a process that transcends local and regional geology is responsible for the formation of these features. If this discontinuity is represented by the base of the cryosphere, its uniform depth over 55° of latitude suggests that the cryosphere did not thicken poleward. Alternatively, the concentration of depths at 1.0- 1.6 km may represent the upper level of non-eruptive dike ascent (lateral dike propagation) of Mars, which is controlled by gravity and atmospheric pressure and magma and country-rock characteristics, and was probably controlled, in part, by ground ice.

Fault-intersection depths in the north Tharsis region locally extend down to a depth of 5-7 km. The depth data between 2-3 km are attributed to the discontinuity at the interface of megaregolith and basement or to the upper limit of non-eruptive dike ascent of magma with a high volatile content. Intersection depths greater than 3 km, which were found at Alba Patera, may be due to the megaregolith-basement discontinuity, which was buried and depressed by volcanic loading, or to the upper level of non-eruptive dike ascent of magma with a low volatile content.

The near absence of narrow simple grabens with fault-initiation depths less than 0.6-1.0 km in this study area, as well as in most of western Mars, suggests that this depth represents the minimum depth that normal faults can initiate; at shallower depths tension cracks or joints would form instead. This hypothesis is supported by the application of the Griffith failure criterion to this minimum depth of normal fault initiation, which suggests that shallow crustal materials have a tensile strength of 2-4 MPa throughout most of western Mars, in close agreement with previous estimates of tensile strength of Martian basaltic rock.

INTRODUCTION

Previous studies have proposed the existence of several mechanical discontinuities within the equatorial region of Mars based on photogeologic observations and topographic data from Mariner and Viking missions (e.g., Sharp 1973a,b; Carr and Schaber 1977; Soderblom and Wenner 1978), on theoretical considerations of the stability of water within the Martian crust and atmosphere (e. g., Smoluchowski 1968; Fanale 1976; Rossbacher and Judson 1981; Clifford and Hillel 1983; Fanale *et al.* 1986), and on analogous impact processes on the Moon and Mars (e.g., Short and Forman 1972; Hörz *et al.* 1976; Aggarwal and Oberbeck 1979; Hartmann 1980; Woronow 1988). These discontinuities include the base of the ridged plains unit, the interface between the debris layer of the megaregolith and the in situ, fractured basement, and the contact bet ween the ice-laden zone and the underlying water-laden or dry zone of impact breccia or between a zone of uncemented, dry impact breccia and an underlying chemically cemented zone. Our previous study of the morphometries of pits, troughs, and wall valleys in the predominantly Hesperian terrain in 1.unae, Syria, and Sinai Plana (Figure 1) indicated mechanical discontinuities at depths of 0.3-0.6 km, 1 km, and 2-3 km (Davis and Golombek 1990). We proposed that the shallowest discontinuity is probably the contact between the widespread ridged plains unit and the underlying megaregolith because the depth corresponds to thickness estimates for the ridged plains unit. The 1-km discontinuity was reflected in the base levels of erosion of all features, as well as in our estimates of intersection depths of graben-bounding faults. Because this discontinuity y has widespread areal distribution and is related to all erosional features thought to have been effected by ground ice or water, we proposed that the discontinuity may represent the base of the ground-ice layer (the interface between ice-laden and dry or water-laden regolith) or the interface between pristine and cemented regolith. We also proposed that the 2-3-km discontinuity, whose depth corresponds to the proposed depth to the base of the Martian megaregolith, is probably the. interface between ejected breccia and overlying in-situ, fractured basement.

Numerous simple grabens and flat-floored erosional feat ures also occur in the Tempe '1'errs and Alba Patera volcanic provinces north of Syria, Sinai, and Lunae Plana. Our current study examines the morphometric characteristics of the flat-floored structural and erosional features that occur in these two north Tharsis regions, whose units have a wide range of geologic ages (Noachian to Amazonian) and occur at high latitudes (30-50° N), in order to investigate the existence of subsurface discontinuities, the latitudinal and temporal variability in the depth of discontinuities most likely related to the cryosphere, the effects of volcanic construct ion (at Alba Patera) on subsurface discontinuity es, and the processes related to graben formation.

The north Tharsis region consists mostly of volcanic (lava and pyroclastic flows) and impact-breccia deposits (Figs. 2 and 3; Wise 1979, Witbeck and Underwood 1984, and Scott and Tanaka 1986; Mouginis-Mark *et al.* 1988; Frey and Grant 1990; Scott and Dohm 1990; Tanaka 1990; Schneeberger and Pieri 1991). The geologic units within the Tempe Terra province are mostly Noachian and Hesperian in age, whereas those in the Alba Patera region are mostly Amazonian in age. Several units within the north Tharsis region contain features that suggest the presence of a water-rich substrate. The Noachian etched unit (unit Nple; Fig. 2) that is exposed in eastern Tempe Terra has irregularly shaped, flat-floored depressions (Fig.

4), which have random orientations and do not appear to be associated with local fault trends. The origin of these depressions has been attributed to thermokarst erosion by melting of ground ice and subsequent collapse of surface material (Gatto and Anderson 1975). The lower (unit Htl) and middle (unit Htm) members of the Tempe Terra Formation have collapse depressions (troughs, pits, pit chains) that are spatially (and probably genetically) associated with faults and fractures (e. g., Mareotis and Tempe Fossa; Figs. 1). The pits are isolated circular to subcircular depressions; the larger pits are generally flat floored (Fig. 5). Pits also occur in chains (Fig. 5) where they generally occur within grabens or parallel local fault trends and, in some cases, adjacent pit rims have coalesced by growth resulting in chains with septate outlines. Troughs are elongated, flat-floored depressions that generally parallel local fault trends (Fig. 5). The ends of scme troughs narrow and have septate outlines, which suggest that troughs represent an advanced stage of pit-chain formation. The flat floors of the troughs and pits in the north Tharsis region may have been controlled by resistant stratigraphic layers or by rapid horizontal erosion and volatilization at the level of the cryosphere or ground-water table (Wise 1979). The absence of debris or of evidence of wind action suggests that material was removed by volatilization, ablation, or subsurface withdrawal. Fretted fracture systems (Fig. 6) occur in the Hesperian ridged plains material (unit Hr; Fig. 2) within Tempe Terra and the Hesperian chaotic terrain (unit Hcht); they also parallel local fault trends. Both terrain types crop out along the south margin of the Tempe Terra plateau (Fig. 2) at the source areas and along margins of channels and may have been produced by disruption of material by volatile release (Scott and Tanaka 1986). In addition to these features there are solitary scarps along the borders of the Tempt Terra plateau that are also bounded by flat surfaces (Fig. 7). The planar appearance. of the surfaces bounding these scarps suggests that the bounding flat surfaces may also represent erosional base levels and, as such, possible mechanical discontinuities.

Other indications of a water-rich substrate in the study areas include: (1) the volcano that occurs within unit Nple in Tempe Terra (Fig. 2), which has obvious radial channels similar in appearance to terrestrial thermokarst topography (Gatto and Anderson 1975); (2) channel dissection (Had; Fig. 3) along the eastern flank of Alba Patera, which has been attributed to sapping due to water release from unconsolidated deposits (Mouginis-Mark et *al.* 1988); and (3) digitate channels and possible lahars in the Ceraunius Fossae region that are areally associated with faults (Tanaka 1990).

Previous studies suggest that the depths of flat-floored depressions (troughs, pits, and irregular depressions) and fretted fractures and the heights of solitary scarps may be related to horizontal mechanical discontinuities in the crust, which may have resulted from strati graphic interfaces, the presence of a water or ice layer, or possibly the presence of a chemically cemented zone in the megaregolith (Sharp 1973a; Soderblom and Wenner 1978; Wise 1979; Rossbacher and Judson 1981; MacKinnon and Tanaka 1989; Tanaka and Davis 1988; Tanaka and Golombek 1989; Davis and Golombek 1990; Tanaka and Chapman 1992). We have obtained photoclinometric profiles across these flat- floored erosional features in the north Tharsis region to determine if their depths cluster and, if they do, whether these depths can be attributed to previously proposed discontinuities.

Faults occur within many of the geologic units within the north Tharsis region. A recent study of the tectonic features of the north Tharsis region separated the faults in Tempe

Terra into eight sets (Scott and Dohm 1990) and the faults in Alba Patera into four stages (Tanaka 1990) based on fault orientation, morphology, cross-cutting relations, and stratigraphic relations. The faults in these two adjacent areas have a dominantly north and northeast trend (Figs. 8 and 9). Most of the faults occur as grabens; they vary in size and morphology, like terrestrial grabens, from narrow, simple grabens to wide, complex grabens. The morphology of the complex grabens display multiple faulted floors and numerous bounding faults, which makes estimation of their fault intersection depths extremely difficult. The morphology of the simple grabens exhibit a simple geometry in which bounding-fault traces are straight and parallel, graben cross sections are symmetric, and graben floors are uniformly flat and unbroken by subsidiary or antithetic faults (Fig. 5). This simple surface geometry implies a simple structure at depth, which suggests that faults bounding simple grabens initiate at a common point at depth and propagate to the surface (Golombek 1979, 1985; McGill and Stromquist 1979; Golombek and McGill 1983).

It has been suggested that the depth of fault initiation for simple grabens is typically controlled by a mechanical discontinuity that separates materials that react differently to extensional stresses (e. g., Golombek 1979, 1985; McGill and Stromquist 1979; Golombek and McGill 1983). This formation mechanism provides a ready explanation for similar widths of grabens within a set or a region, which may be difficult to explain otherwise (see Melosh and Williams 1989 for an alternative mechanism for graben formation). In either case, topographic profiles across these grabens can be used to determine the depth below the surface at which faults bounding simple grabens intersect (assuming a fault dip). If fault intersections cluster at particular depths, they can be used to infer the depth to a mechanical discontinuity, especially if the intersection depths coincide with observed depths of proximal flat-floored erosional features that may be the surface expressions of the discontinuities.

We have obtained morphometric data for most of the simple grabens in the Tempe Terra and Alba Patera regions; we use these data to estimate the depths of fault intersection, which are in turn used to evaluate the factors that may have controlled fault initiation of the simple grabens in this region of Mars. The grabens for which we have collected data occur within most of the major recognized geologic units at Alba Patera and Tempe Terra and occur over a wide range in elevation (from 3 to 7 km) and latitude (from 29° N to 55° N); as such, this data set is more extensive than the east-west transect examined by Plescia (1991). Therefore, these data allow an examination of the possible effects of local stratigraphy (including the basement), thickness of the volcanic pile at Alba Patera (inferred from topography), and possibly, depth to the base of the cryosphere (which is the crustal zone where the temperature is continuously below the freezing point of water; theoretical models suggest that the depth of this zone's lower boundary may increase towards higher latitudes).

PHOTOCLINOMETRY

Topographic profiles across flat-floored structural and erosional features were generated using the symmetric and asymmetric methods developed by Davis and Soderblom (1984) and using calibrated Viking Orbiter clear- and red-filter digital images. Both methods use a photometric function, knowledge of the solar incidence (i) and spacecraft emission (e) angles and their azimuthal angles, and an estimate of atmospheric scattering to determine the slope of each pixel along a designated profile. We used the Minneart photometric function (Minneart 1941) of the form $B = H + SB_o (\cos i)^k (\cos e)^{k-1}$, where B is the measured brightness of a pixel; H is a constant and is the additive effects of atmospheric scattering (haze); S is a constant and represents the combined effects of solar flux, attenuation by atmospheric scattering, camera sensitivity, and exposure time; B_o is the surface albedo; and k is the Minneart coefficient that varies with phase angle. We used the relation $k = 0.0062\alpha + 0.45$ (Tanaka and Davis 1988) for clear-filter Viking Orbiter images, where α is the phase angle of the image; we used the tabulated values of k versus α from Thorpe (1973) for red-filter Viking Orbiter images. An estimate of haze for each image used in this study was obtained from shadows either within the image (if there were shadows) or within images that have shadows that were acquired near the study image in space and time.

"The symmetric method uses two opposing profile lines (one downsun and one upsun) along which changes in topography and surface albedo are judged to be symmetric to a first order. Brightness values (corrected for haze) along both profile directions are ratioed pixel-by-pixel, starting at their common endpoints, which results in a relation that is only dependent of surface orientation. The asymmetric method is similar to most photoclinometric methods that have been used in recent years (e.g., Jankowski and Squyres 1992) in that an estimate of the brightness of a flat surface must be estimated and the albedo along the single profile must remain constant in order to obtain a valid solution. The relative constancy of the albedo is judged by applying a linear contrast stretch to the image on an interactive display. Because the solution is very sensitive to the albedo value, results from this method have higher error than those from the symmetric method, Therefore, wherever possible, we used the symmetric method, which we employed on the grabens, pits, troughs, and fretted channels. The asymmetric method had to be used for the irregular depressions and solitary scarps because they did not have symmetric topography or they did not have an opposing slope. Both of the photoclinometric algorithms used in this study take into account oblique viewing geometry during their iterative process.

There are five main sources of error in these photoclinometric methods: radiometric calibration of the image, estimation of the haze value (H), estimation of the albedo of a flat surface (B_o), estimation of the photometric constant (k), and orientation of the profile relative to topographic strike and the maximum solar scattering plane (the solar azimuth). Different viewing and lighting conditions result in differences in the sensitivity of photoclinometric measurements, which are difficult to predict *a priori* (Davis and McEwen 1984; Jankowski and Squyres 1991). Therefore, our algorithms repeat a profile's calculation using reasonable estimates of the uncertainties associated with image calibration, haze, brightness of a flat surface, and photometric constant; the difference between the two solutions is an estimate of the error for each pixel in the profile. We used an average uncertainty of +2-3% for the calibration, ±0.05 for the Minneart coefficient, and ±5% for the brightness of a flat area.

The amount of atmospheric scattering on Mars varies with time and location. We avoided images acquired near Martian dust storms because the high amounts of haze reduce the signal and increase the error associated with haze removal. We used red-filter images from Viking Orbiter 1 revs 519, 520, 555, 558, and 858 and clear-filter images from Viking Orbiter 1 revs 627, 667, 668, 1253, 1254, 1255, 1256, 1257, and 1258. The measured haze (in 16-bit DN) for the red-filter images ranged from 350-625 with an average uncertainty of about 9%, whereas the measured haze for the clear-filter images ranged from 330-430 with an average uncertainty of about 4%. On average this level of uncertainty in haze results in an measurement error of about 7%-12 % in both methods. When uncertainties in calibration and k are included, the cumulative error is about 12%-18%. The added uncertainty in estimation of flat-field brightness (for the asymmetric method) increases the total measurement error to as much as 24 % in some cases.

The principles of photoclinometry require that profiles be obtained perpendicular to surface slope. There are many instances for the north Tharsis region where images do not exist in which a surface's strike is perpendicular to solar azimuth. "1'bus, profiles had to be obtained at an angle to solar azimuth. In fact, the average graben measurement was obtained at an angle of 32° from the solar azimuth and the average scarp measurement was obtained at angle of 210 from the solar azimuth. An estimate of the error associated with nonazimuthal profile lines was determined by profiling bowl-shaped craters within several study images using average uncertainties for haze, k, calibration, and brightness of a flat surface, varying the profile azimuth in increments of 5°, and noting the difference in integral height. The results indicate an average cumulative error of21 % for the symmetric method and 24% for the asymmetric method.

PHOTOCLINOMETRIC RESULTS

The locations of the topographic profiles that we generated across solitary scarps, troughs and pits, fretted fractures, and irregular depressions are shown by closed circles in Fig. 2; the profiles across the simple grabens are shown by the closed circles in Figs. 8 and 9. We obtained replicate measurements on 30 features in which each feature occurred on 2-3 images; the deviations (1 σ) in these replicate measurements were 4.5 % for width, 12.2 % for depth, and 17.8% for slope. The number of measurements within each geologic unit was limited by the number of structural and erosional featu es in each unit and by the slope orientation of the features with respect to the solar azit nuth of Viking Orbiter images (i.e., we did not obtain data on features whose slope required a profile more than 45° from the solar-azimuth angle because of the high error associated wit] ı such profiles). From each profile we extracted depth or 'height, wall slope, and rim-to-rim width.

We obtained photoclinometric profiles across 10 irregular depressions, 32 fretted fractures, 49 troughs and pits, and 124 solitary scarps within the Tempe Terra region of Mars (closed circles on Fig. 2). The average slope and height of the solitary scarps and the average depth, wall slope, and rim-to-rim width of the troughs and pits, fretted fractures, and irregular depressions are listed in Table I. For the larger troughs and ii-regular depressions that vary in in width or depth, we obtained profiles at different locations along each feature and calculated their average width or depth. The frequency distribution of measured depths or heights for each type of feature is shown in Fig. 10; the fı equency distributions of measured heights and depths for all of these features, separated by the geologic unit in which these measured features occur, are shown in Fig. 11.

We also obtained photoclinometric profiles of 198 simple gıabens within Tempe Terra and 172 simple grabens within Alba Patera (closed circles on Figs. 8 and 9, respectively). The average slope, depth, and rim-to-rim width of each graben set and stage defined by Scott and Dohm (1990) and Tanaka (1990) are summarized in Table II. We obtained multiple profiles along 62 of the larger graben segments; the average deviations (1 σ) in their measured morphometries are 8.8% for rim-to-rim width, 18.6 % for depth, and 17.770 for wall slope. The wall slopes of the simple grabens in this study area are generally less than 10° (Table II), which implies that the wall slopes have been lowered by mass wasting, similar to that found for the grabens in Syria, Sinai, and Lunae Plana (Tanaka and Davis 1988; Davis and Golombek 1990). In order to accurately estimate the intersection depth of each set of graben-bounding faults, it is necessary to estimate the original width of each graben by removing the effects of mass wasting (e.g., Golombek 1979; Tanaka and Davis 1988; Davis and Golombek 1990), which was not considered by Plescia (1991). Mass wasting has a significant effect on graben width; reduction of a graben's wall slope from 60° to 10° results in a 30 to 50 percent increase in its width. Thus, if the effects of mass wasting are not numerically considered, the fault intersection depth will be overestimated by a factor of about 1.3 to 2.

The dip of the faults must be known in order to accurately remove the effects of mass wasting on the graben walls (the dip of the faults is the initial slope of the graben walls). We examined all Viking Orbiter images for Tempe Terra and could not find reliable fault traces on any of the images that would allow a three-point determination of fault dip (such as the procedure described in Davis and Golombek 1990). There is a linear trace on the western scarp of Tempe Terra (about 8 km south of profile B on Fig. 5), which we determined to have a dip of 63.8° by the three-point analysis described in Davis and Golombek (1990). However, we are not confident that this is a fault-plain trace. The trace is associated with a graben, but the graben appears to have been eroded; hence the trace may be a secondary or depositional feature. In our analysis of mass wasting and fault-intersection depth, we assumed the average fault dip (60°) that we obtained by direct measurement of five fault-plane traces that intersect trough walls in Sinai Planum (Davis and Golombek 1990). This assumption is probably valid because the gross geologic units within the north Tharsis region and in the plana to the south are thought to be similar in 1 itholog y (although different in age; Scott and Tanaka 1986) and because fault dip is not strongly influenced by lithologic type (see discussion and references in Davis and Golombek 1990). We used this fault dip value and the rim-to-rim width, depth, and wall-slope data for each graben and the method of Golombek (1979) to estimate the fault-intersection depth for each simple graben that we profiled (Table II).

The frequency distributions of the fault-intersection depths in the Tempe Terra and Alba Patera regions are shown in Fig. 12 as percentages of each measured population. The fault-intersection depths in Tempe Terra have a range between 0.3 and 4.8 km, a mode centered at the 1.0- 1.2 km interval (Fig. 12), and an average of 1.4 ± 1.2 km (Table II). In contrast, the fault-intersection depths in Alba Patera (Fig. 12) have a range between 1 and 7 km, a broad mode between 1.2 km and 2.0 km, and an average of 2.8 km ± 1.7 km. These data for both regions exhibit a sharp drop off at shallow depths, characteristic of a Poisson distribution. This drop off is not an observational bias because the narrowest simple graben found in the Alba Patera area is wider than the narrowest graben that potentially could be discerned and photoclinometrically profiled using the available Viking Orbiter images. Thus, the steep drop off in frequency of fault-intersection depths less than 1 km at Alba Patera is not the result of limitations in either the image data or the photoclinometric method, but represents a real dearth of very narrow simple grabens with shallow fault intersection depths.

DISCUSSJON

Within the north Tharsis region some possible mechanical discontinuities include lithologic interfaces between lava flows, cratered and fractured materials composed of impact breccia and lava flows, possible sills, and, within the Alba Patera region, pyroclastic flows (Wise 1979; Scott and Tanaka 1986; Mouginis-Mark et al. 1988; Schneeberger and Pieri 199 1). The existence and depths of these lithologic discontinuities may vary locally because of differences in local geologic history. The heights of the solitary scarps that we measured provide clues to the depths of these discontinuities and possibly the depth to the top or base of the cryosphere in this region.

The Martian megaregolith is generally 'considered to be volatile rich based on estimates of the amount of water that may have been involved in geologic processes [in terms of a global water layer these estimates range from 46 m (Greeley 1987) to greater than 500 m (Carr 1986)] and the high volatile content of meteorites from Mars (Dreibus and Wänke 1985). The amount of water at the Martian poles and in the atmosphere accounts for only a small fraction of these estimates (Farmer *et al.* 1977; Carr 1986); the amount of water lost from the atmosphere is also estimated to have been very small (Walker 1977). Clifford (1993) presented impact scaling data for Mars that suggest the. megaregolith has significant porosity and total pore space to accommodate a global water layer 0.5- 1.5 km deep.

Theoretical considerations of the thermal diffusion properties of the Martian regolith and atmosphere suggest that (1) ice is not stable near the surface between ±40° latitude, although small pockets of ice may exist within the equatorial region at shallow depths; (2) if significant amounts of ground ice do exist in the equatorial region, a continuous or periodic process of replenishment may be required; (3) the upper few meters of the regolith may retard diffusion in the equatorial region and protect the ground ice or water, especially if a shallow, chemically cemented layer exists; (4) the cryosphere increases in thickness (depth) from km between ±30° latitude to as much as 3 km at the poles; (5) ground ice. is stable at the surface above 40° latitude, which is probably transitional and initiates at some shallow depth below 40°; and (6) beneath the ground ice layer water may exist due to geothermal heating of the base of the ice-laden zone (Fanale 1976; Soderblom and Wenner 1978; Rossbacher and Judson 1981; Clifford and Hillel 1983; Fanale et al. 1986; Paige 1992; Mellon and Jakosky 1993). The presence of landforms indicative of terrain softening (due to the presence of ground ice) above 40° latitude and their near" absence within ±30° latitude agrees with these theoretical calculations (Squyres and Carr 1986). Theoretical modeling of the morphometries of craters that are indicative of terrain softening suggests that the ground ice layer has a thickness of 1 km between 30-40° latitude, which is also consistent with theoretical calculations (Jankowski and Squyres 1992).

Considering these previous studies, potential widespread mechanical discontinuities that involve the cryosphere could exist in the north Tharsis region and could include interfaces between ice-laden and dry regolith, ice-laden and water-laden regolith, and pristine and chemically cemented regolith. The grabens and erosional features measured in this study occur within the zone of increasing thickness of the cryosphere and shallowing surface stability of ground ice. Thus, their morphometries may reflect the depths to the possible discontinuities associated with ground ice and water. Another discontinuity that probably exists throughout the north Tharsis region is the interface between the impact brecciated megaregolith and the basement (Fanale 1976; MacKinnon and Tanaka 1989); the thickness of the Martian megaregolith has been estimated to be about 2-3 km (Fanale 1976; Woronow 1988). The graben-bounding faults provide the deepest probes for mechanical discontinuities, thus some fault-intersection depths may be at the base of the megaregolith. The discussion that follows considers the morphometric data in the order of shallowest to deepest discontinuities that the depths of the features may represent.

Solitary Scarps-Lithologic Discontinuities

Frey and Grant (1990) obtained estimates of the maximum thickness of the heavily cratered and ridged plains terrain within Tempe Terra using the diameter of the largest, mostly buried craters and the depth-diameter relation for fresh Martian craters of Pike and Davis (1984). hey estimated that the heavily cratered terrain (corresponding to units Nple and Npl_1; Fig. 2), has experienced about 460 m of resurfacing. Their estimated maximum total thickness of the ridged plains terrain (corresponding to unit Hr; Fig. 2) was 562 m within Tempe Terra (Frey and Grant 1990) and 660 m within Lunae Planum (DeHon 1985). The thickness values obtained for these units by Frey and Grant (1 990) and DeHon (1985) are close to the modes in the frequency histograms of our measured scarp heights within these units (Fig. 11), but our measured heights of many of these unit scarps exceed the previously estimated "maxmimum" thickness values. Assuming that the maximum thickness estimates of Frey and Grant (1990) and DeHon (1985) are correct, the observed modes in our frequency histograms are more representative of unit thicknesses than are the largest scarp heights that we measured in each unit. If this relation is correct, the frequency modes of our scar-p-height distributions suggest that the thicknesses of most of the exposed geologic units in Tempe Terra are less than 600 m (Fig. 11).

The larger scarp heights within each geologic unit may represent the cumulative thicknesses of underlying strata that may have been exposed by uplift and erosion. It has been suggested that some of the scarp heights within units Nb, Nplh, and Npl_1 units have been produced by uplift (by normal faulting) and tilting (Scott and Tanaka 1986). Similarly, the scarp heights within unit Hr that are greater than 1 km were obtained along the southern margin of the Tempe Terra plateau, which also may have been affected by uplift and also by erosion of Kasei Vanes, and thus these larger scarp heights may also represent the cumulative thickness of underlying strata.

Irregular Depressions, Fretted Terrain, and Pits and Troughs -Cryospheric or Lithologic Discontinuities

Overall, the range in depths of Tempe Terra features whose origins may be directly related to ground ice increases in the order of irregular depressions (55-175 m), fretted fractures (85-890 m), and troughs and pits (60-1,620 m) (Fig. 10). The irregular depressions occur within the Noachian etched plateau unit (Nple) in eastern Tempe Terra, the fretted fractures occur within the Hesperian ridged plains unit (Hr) in southern Tempe Terra, and the troughs and pits occur mostly within the lower and middle members of the Tempe Terra Formation (Htl and Htm) in western Ternpe Terra (Fig. 2). This observation by itself might suggest that the thickness of or the depth to the Martian ground ice. increased with time. However, these depressions formed roughly within the same timeframe (Late Hesperian to Early Amazonian; Scott and Tanaka 1986). It is more likely that this observed relation is the result of either a thicker stratigraphic column over the ice-laden zone where younger rocks exist or an increased efficiency in the removal of material by the hydrologic systems when joints and especially faults are involved (as they were in the formation of fretted fractures, pits, and troughs).

If the thickness of the cryosphere increased poleward ancl the floors of the fretted fractures, pits, and troughs correspond to the base of the ground ice, then the depths of these flat-floored features should be greater in Tempe Terra than in adjacent equatorial regions. The floor depths (1.2- 1.6 km) of the larger troughs in western Tempe Terra are similar to, but not greater than those of the large troughs to the south in Syria and S inai Plana (Davis and Golombek 1990). In addition, most of the floor depths of the pits and troughs in Tempe Terra (average depth is *374 ± 357* m; Table 1) are much shallower than those in Syria and Sinai Plana (average depth is 1,712 ± 734 m; Davis and Golombek 1990). Thus, if the floors of these features correspond to the base of the ground ice, our depth data for these features suggest that the ground-ice layer thins poleward, which is contrary to theoretical models (Fanale 1976; Rossbacher and Judson 1981; Fanale *et al.* 1986). Alter natively, the floor depths of the pits and troughs in Tempe Terra may be related to stratigraphy or may (for the shallower pits and troughs) correspond to the top of the ground-ice layer, which may have been stable at increasingly shallower depths in the Martian crust toward the poles. Another possibility is that the development or existence of Vanes Manneris, which is significantly deeper than any other erosional feature in Syria and Sinai Plana, affor ded anomalously deep erosional base levels to be achieved (for the central latitudes) in the depressions that surround the canyon system, The depth range of the fretted fractures within Tempe Terra (0.2- 1.0 km; Fig. 10) is similar to that obtained for the fretted fractures in Sacra Fossae (0.2-1.3 km; Davis and Golombek 1990). As in Sacra Fossae, the fretted fractures in Tempe Terra are shallowest at fracture heads and deepen toward fracture mouths that open onto Kasei Vanes. The maximum depths of the fretted fractures appear to be controlled by the height of the Tempe Terra plateau above the erosional base level of Kasei Vanes (Figs. 6 and 7). Similarly, the shallow irregular depressions in eastern Tempe Terra (Fig. 4) debouch onto multiple, common plateau and plains levels and appear to be stratigraphically controlled. A nearby circular structure surrounded by radiating tongue deposits (at lat. 46° N, long. 55.5°; Scott and Tanaka 1986) may be volcanic and may have been the source of hydrothermal activity that resulted in sapping and formation of the irregular depressions.

The depths of the irregular depressions, fretted fractures, troughs, and pits are close to the frequency modes of the solitary scarp heights for the units that are areally associated with the depressions (Fig. 11). This observation suggests that the development of most of the depressions was controlled by lithologic interfaces that were resistant to erosion and downward removal of material along joints and fractures by ground water/ice, as previously suggested by Wise (1979). The one exception to this correspondence between depression depths and scarp heights are the large troughs that have depths (1.2-1.6 km) greater than the measured scarp heights of unit Htl in which they occur (Fig. 11), However, the depths of these large Tempe Fossae (northeast-trending) troughs are very similar to the scarp heights of the older Mareotis Fossae (north-trending) troughs (1.2-1.8 km; profiles A, B, and C in Fig. 5) and to the heights of northern (Npl_1) and southern (Hr) border scarps of the plateau (Figs.

2 and 11). Thus, the depths of these larger troughs may be indicative of the cumulative thickness of subjacent lithologic units in western Tempe Terra and possibly an equilibrium base level of erosion for this area or may be indicative of the base of the ground-ice layer. The widths of most Tempe Fossae troughs narrow to the northeast, which suggest that material mobilized in the troughs and pits moved mostly westward, probably along subsurface fracture systems. The most pronounced surface manifestation of this is the longest Tempe Fossae trough (labeled D on Fig. 5) that extends for about 70 km, along which the trough widens and deepens southwestward, cuts through the north-trending uplifted plateau scarp, until it reaches the base level of the old Mareotis Fossae troughs.

Faulting assisted in the formation of the fretted fractures, troughs, and pits (Sharp 1973b; Schumm 1974; Baker and Kochel 1979; Kochel and Burgess 1982; Schultz 1989; Tanaka and Golombek 1589; Lucchitta *et al.* 1990). The rectangular pattern exhibited by the fretted terrain (Fig. 6) has led to the suggestion that these fractures were joint controlled (Sharp 1973b; Schumm 1974; Kochel and Burgess 1982; Tanaka and Golombek 1989) and that jointing increased permeability and caused mass wasting and sapping by groundwater or ground ice. The troughs and pits present a variation on this scenario because these features are closed depressions and require either sublimation, ablation, or subsurface drainage to remove the missing material. Subsurface drainage is currently believed to be the most likely scenario because the amount of water necessary under the pure sublimation hypothesis would require an upper crust largely made up of ice (Sharp 1973a; Schultz 1989; Lucchitta *et al.* 1990) and there is no evidence of wind action in the depressions (Wise 1979). Some of the troughs and pits in the study area and in adjacent areas display two levels of development

(Wise 1979; Davis and Golombek 1990), which has led to the suggestion that trough and pit development is controlled either by (1) stratigraphy in which horizontal erosion operates on successively deeper lithologic interfaces, or (2) re-equilibration of the ice-laden zone's depth with respect to the surface in which trough and pit development ceases at the original depth of the ice-laden material and resumes at a new deeper level (Wise 1979).

Fault-intersection Depths-Lithologic, Cryospheric, or Megaregolith Discontinuities

Another indirect indication of the depths to mechanical discontinuities in the north Tharsis region is the intersection depths of graben-bounding faults, which we estimated using the surface morphometry of the simple grabens that occur in this region and the assumed 60° dip of the faults. The mode in the frequency histogram of the fault-intersection depths for the Tempe Terra region is 1.0- 1.2 km (Fig. 12). This mode in fault-intersection depths is close to the depth values for the larger troughs (1.2- 1.6 hn) within the Htl unit and the 1-2 km heights of plateau border scarps in the Hr, Npl_1, and Nb units (Fig. 11). A comparison of fault-intersection depths, depression depths, and solitary scarp heights within different geologic units (Figs. 11 and 13; Table IIT) shows that, although there is overlap in these frequency distributions for units Npl_1, Hr, Htl, and Htm, most of the fault-intersection depths are greater than the depression depths and scarp heights in each geologic unit. Thus, most of the graben-bounding faults in Tempe Terra originated at mechanical discontinuities that have generally not been exposed at the surface. We cannot make a similar comparison at Alba Patera because there are no scarps to measure the thicknesses of the geologic units that occur in that region.

The frequency distribution of fault-intersection depths within Tempe Terra shows a small population of depths greater than 2 km (Fig. 12), which were also found in Syria, Sinai, and Lunae Plana (Davis and Golombek 1990). The fault-intersection values between 2-3 km probably represent the megaregolith-basement interface. The few fault-intersection depths in excess of 3 km could represent local depressions of the basement due to localized burial by volcanics of the Tempe plateau or they may represent the depths to the tops of deep-seated dike intrusions.

The average fault-intersection depth of Alba Patera (2.8 ± 1.7 km) is significantly greater than that of Tempe Terra (1.4 ± 1.2 km) and Syria, Sinai, and Luna Planae (1.5 ± 1.0 km). In addition, the frequency distribution of fault-intersection depths for Alba Patera has a broader mode and extends to greater depths than these other regions. This is probably the result of Alba Patera's unique geologic setting relative to these other regions. Because of the patera's obvious constructional nature we examined the distribution of fault-intersection elevations versus the distance that each fault-intersection depth measurement is from the summit of Alba Patera (Fig. 14). We calculated the elevation of each fault-intersection measurement using each site's calculated fault-intersection depth and reported surface elevation (U.S. Geological Survey, 1989). This distribution (Fig. 14) shows that the intersection depths of graben-bounding faults (1) exhibit a lower limit of about 1 km, (2) occurred at increasingly greater depth ranges toward the summit of Alba Patera (where the depth range is approximately from 2 km to 7 km), and (3) only occurred below the O-km reference elevation within 700 km of the summit (except for a single fault-intersection depth obtained in a Noachian unit in the far eastern border of the study area; Figs. 3 and 14).

The data for the eastern half of Alba Patera show a continuum of graben-bounding faults originating from depths of 2 to 7 km near the summit, unlike the data obtained along a transect across southern Alba Patera (Plescia 1991), which showed an absence of graben-bounding fault intersections at shallow depths (< 3 km) near the patera's summit (Fig. 14). As suggested by Plescia (1991), one possible reason for the gradual increase in the depths of graben-bounding faults towards the patera's summit is the depression of the interfaces between the megaregolith and basement from volcanic construction, burial, and subsidence during the formation of the patera. The continuum of fault-intersection depths may represent, at least *in* part, mechanical discontinuities between volcanic (lava and pyroclastic flows), interbedded regolith, plutonic units, and possibly an ice-laden zone.

The concentrations of fault-intersection depths at 1.0- 1.2 km for Tempe Terra and at about 1.2- 1.6 km for Alba Patera are very close to the 0.8- 1.2-km mode observed in the fault-intersection depth data for areas that we have examined within the western equatorial region of Mars (Syria, Sinai, and Lunae Plana; Davis and Golombek 1990). in fact, the frequency distributions of fault-intersection depths for Tempe Terra and the three plana are remarkably similar. The fault-intersection data for all five areas, which cover a latitude range from 15° S to 55° N, do not show a marked increase in depth towards higher latitude. The consistency in the frequency modes of the fault-intersection depths within the western hemisphere of Mars suggests either (1) the base of the ground-ice layer does not begin to thicken poleward until higher latitudes (>55° N); (2) the theoretical poleward thickening is masked by other discontinuities; (3) local variations in ground-ice thickness, due to a variety of factors, mask broader regional trends within this latitudinal band; or (4) these similar modes in fault-intersection depths may indicate that a large fraction of the graben-bounding faults originated at the top of ground-ice layer, whose depth may not become appreciably more shallow at these latitudes. A first-order, thin-layer relaxation model of "softened" craters that occur at the latitudes of Tempe Terra (but about 135° to the east) suggests that the ice-laden zone is about 1 km in thickness (Jankowski and Squyres 1992). This result indicates that the first scenario, although contrary to theoretical diffusion calculations (Rossbacher and Judson 1981; Fanale 1976; Fanale et *al.* 1986), may be possible. Even though the latitude that the cryosphere begins to thicken at a particular longitude may vary due to regional variations thermal inertia of the regolith (Mellon and Jakosky 1993), the absence of "terrain softening" features within ± 30° latitude suggests that the fourth scenario is more. probable than the first scenario.

Fault-intersection Depths-Lateral Dike Propagation Alternative

Another explanation for the consistency in the frequency modes of graben fault-intersection depths within Tempe Terra, Alba Patera, and previously studied equatorial regions is that the 1.0- 1.6 km depths may represent the upper limit of non-eruptive dike ascent on Mars. On Earth, dikes are typically associated with grabens in volcanic terrains (e.g., Gibson *et al.*, 1987; Mastin and Pollard 1988; Rubin and Pollard 1988). The areal association between planetary volcanic centers and grabens has led to the suggestion that propagating dike systems ate a viable mechanism for graben formation on the Moon (Wilson and Head 1981), Venus (McKenzie *et al.* 1992; Parfitt and Head 1993), and Mars (Tanaka and Golombek 1989; Schultz 1989). Photogeologic evidence of lava flows and small volcanoes emanating from several grabens and fissures around Tempe Terra (Moore and Hodges 1980; Plescia 1981; Tanaka *et al.* 1991; Davis and Tanaka 1993) and of lava flows emanating from several grabens and fractures around Alba Patera (Schneeberger and Pieri 1991) suggest that dikes may have produced at least some fraction of the grabens in these regions.

Studies of terrestrial dike systems have shown that dike ascent is controlled by several factors related to the characteristics of the magma and country rock (e.g., Pollard 1976; Wilson and Head 1981; Rubin and Pollard 1988; Lister 1991; Parfitt 1991). The level of dike ascent on any particular planet is also dependent on a planet's gravity and atmospheric pressure (Wilson and Head 1994). Previous theoretical studies, based on estimates of terrestrial magma and country-rock characteristics, have indicated that dikes will ascend to the level of neutral buoyancy and then propagate laterally near this level until they erupt or their driving pressures decline (e.g., Lister 1990, 1991). An analysis of the Krafla rift zone by Rubin (1992) suggested that grabens form in front of and above laterally propagating dikes.

Parfitt and Head (1993) modeled the emplacement of lateral dikes under conditions of constant and declining driving pressure conditions. Their results using constant driving pressure conditions show that dikes will grow vertically and laterally until they intersect the surface ($\leq$ 100 km from the chamber) and produce long, voluminous flows or until they reach a stable vertical height (level of neutral buoyancy) and grow laterally (up to several thousand kilometers) at that height until stopped by cooling or pressure loss. They suggest that caldera collapse may be associated with the later stages under these conditions because the magma chamber could drain to a point where reduced magma pressure would result in roof failure. In contrast, declining driving pressure conditions produce dikes of more limited width (<4 m), lateral extent ($\leq$ 100 km), and height, which results in dikes of finite, fairly consistent length (determined by the volume of the magma chamber) that usually do not erupt unless they are very shallow.

If the simple grabens in north Tharsis were produced by dike intrusion, several characteristics of these grabens suggest that the dikes were more likely to have propagated under a constant driving pressure than under a declining driving pressure. First, the simple grabens show a wide range in lengths (from about 50 km to 400 km) with a large fraction of the simple grabens having lengths $\geq$100 km, larger than that expected from dikes under declining pressure conditions. Second, as stated above, previous studies have noted the existence of lava flows emanating from several grabens in Tempe Terra and Alba Patera. Third, Alba Patera has a summit caldera, consistent with the Parfitt and Head (1 993) model for dike systems under constant driving pressure conditions. Fourth, our estimates of the widths of the dikes that may be associated with the simple grabens (based on the relation of extension and dike width of Mastin and Pollard 1988) range from 150-450 m, which is significantly wider than dike widths proposed under declining pressure conditions.

There are a few advantages of the lateral dike propagation hypothesis over other possible explanations of the graben-bounding, fault-intersection depth data for western Mars. First, several factors involved in a dike propagation model vary spatially and temporally with respect to the associated magma chambers, which could account for the range of fault-intersection depths that we find within different study areas in north Tharsis. For example, the decrease in fault-intersection depths from the summit to the eastern base of Alba Patera, as well as the paucity of fault-intersection depths greater than 2 km at distances greater than

700 km from the summit (Fig. 14), could be explained by a transition from predominantly vertical dike ascent near the summit to predominantly lateral dike movement at some distance from the magma chamber. In fact, the 700-km distance from Alba's summit corresponds closely to the 500-600-km distance found by Ernst and Baragar (1992) for the transition from vertical to horizontal dike movement in the Mackenzie dike swarm. Second, the hypothesis can explain observable geologic and spatial relations between volcanic deposits, tectonic features, and hydrologic features in the study areas. Even though this hypothesis would not depend on a uniform, planetwide stratigraphic or cryospheric interface to explain the uniformit y in frequency modes (1.0- 1.6 km) of the fault-intersection depths, it would require the presence of a volatile-rich layer in order to arrest dike ascent at these shallow fault-intersection depths on Mars. Wilson and Head (1994) estimated the neutral buoyancy level for Earth and Mars based on a pressure volubility law and estimates of surface void fractions. Their estimate for Earth's neutral buoyancy level (3 km) is within the range observed beneath Kilauea (2.5-4.5 km; Ryan 1987). Their results for Mars suggest that the level of neutral buoyancy is at a depth of 11 km, which is deeper than the 7.7 km depth based on gravity scaling alone. Assuming that the Martian level of neutral buoyancy is 7.7-11 km for a volatile-free magma, lateral dike propagation at the shallow depths of 1.2- 1.6 km (suggested by fault-intersections depths) would require the existence of volatiles in the magma.

Wilson and Head (198 1) calculated that magma on Mars, with sufficient driving pressure and with typical H_2O or $C0_2$ content in the source region, would be expected to reach a gas volume fraction of 0.75 by volatile exsolution at depths of less than about a kilometer, resulting in eruption. (The depth at which this gas volume fraction is achieved, i.e., the "fragmentation depth," will vary depending on magma silica content, volatile content, and temperature and on the density profile of the crust.) Based on estimates of the depth dependence of gas-bubble and magma fragmentation on magma H_2O content in a Martian environment (Wilson and Head 1994), magma with 1-3 % H_2O (which is not unreasonable for Mars) would have neutral buoyancy at a depth of about 1-2 km. Thus, magmas having lower driving pressures and sufficient volatiles may instead spread laterally at depths of 1 km or greater, resulting in extension, graben formation, and possibly sill formation. The presence of an ice-laden zone in the megaregolith of western Mars could also inhibit dike ascent due to quenching of the magma and contribute to lateral spreading of dikes, which could result in extension and graben formation, and possibly sill production (intrusion into wet sediments on Earth generally results in a sill (Kokelaar 1982)).

Regardless of the exact mechanism of graben formation (in fact, both dike propagation and non-volcanic tectonic extension may have produced grabens under different conditions or areas of Mars), the sparsity of very narrow simple grabens with fault-intersection depths less than 0.6- 1.0 km (Fig. ~~11~~ 12) can be used to place constraints on the maximum depth of tensile cracks on Mars under typical conditions. Grabens, which are bounded by normal faults, are indicative of shear failure that occurs when rocks fail under extensional stresses at depth. Tension cracks or joints form under similar extensional stresses at shallow depths where overburden is low. The minimum depth at which normal (shear) faults can initiate is the maximum depth at which tensile failure can occur, which is limited by the overburden stress and the tensile strength of the material under the Griffith failure criterion for intact rock (Tanaka and Golombek 1989) or under Hock-B~own criterion for jointed rock masses (Schultz

1993). For minimum depths of shear failure of 0,6- 1.0 km, shallow crustal material must have tensile strengths of at least 1 - 4 ~~2-4~~ MPa under dry or hydrostatic conditions. These tensile strengths are well within the range of expected tensile strengths for the types of materials expected in the shallow crust on Mars (Tanaka and Golombek 1989), particularly for basaltic rock masses (e.g., 1-6 MPa, Haimson and Rummel 1982; <2 MPa, Schultz 1993). In addition, crack spacing measurements in Iceland suggest a maximum terrestrial fracture depth of $\leq$400 m (Opheim and Gudmundsson 1989); this value, properly scaled for gravity, would suggest a maximum fracture depth of about 1 km on Mars. The fact that the sharp drop off in narrow grabens with shallow fault intersection depths is evident throughout the western hemisphere of Mars (e.g., Davis and Golombek 1990) argues that tensile strengths of this magnitude are prevalent for shallow crustal rocks over most of the red planet,

CONCLUSIONS

Photoclinometric measurements of 91 flat-floored depressions, 124 solitary scarps bounded by planar surfaces, and 370 simple grabens (from which we estimated fault-intersection depths) provide indirect evidence of mechanical discontinuities and constrain possible mechanisms for graben formation in the north Tharsis region of Mars. The following summarizes our findings from an examination of these data.

1. The modal heights of measured solitary scarps (bounded by planar surfaces) within the heavily cratered and ridged plains terrain in Tempe Terra correspond closely to previous thickness estimates of these units. The modal depths of measured flat-floored depressions also correspond to the modal heights of measured solitary scarps within all of the geologic

units in which these features occur, which suggests that stratigraphy was a major controlling factor in the development of the depressions. The uniformly shallow height and depth modes of the scarps and depressions (<0.8 km) throughout the entire region, irrespective of geologic unit, and the previously proposed hydrologic influence on the development of these depressions suggest that the top of the ice-laden zone may have been another primary factor controlling the development of these features. The large flat-floored troughs in western Tempe Terra reach depths of 1.2- 1.6 km, which is similar to scarp heights along the margins of Tempe Terra plateau; their formation may have been controlled by the base of ice-laden rock.

2. Fault-intersection depths in Tempe Terra and Alba Patera also show a concentration of data at 1.0- 1.6 hn. Trough, pit, and faulted-layer depths obtained from Syria, Sinai, and Lunae Plana also show a concentration of data very close to this depth interval. The consistency of these data over such a large region of western Mars suggests that a discontinuity or a process that transcends local and regional geology is responsible for the formation of these features. The most frequently cited widespread discontinuity on Mars is the cryosphere. However, the uniformity of our depth data over 55° of latitude suggests that the cryosphere did not thicken poleward, which is contrary to theoretical models. Alternatively, the concentrate ion of depth data at 1.0- 1.6 km in these different regions of western Mars may represent the upper level of non-eruptive dike ascent on Mars (i. e., the level of neutral buoyancy), which is controlled by magma and country-rock characteristics and gravity. This shallow depth range suggests that dike ascent was confined by the presence of a ground-ice layer beneath the surface.

3. The frequency histograms of fault-intersection depths extend down to a depth of 4 km within Tempe Terra and 7 km within Alba Patera. The fault-intersection depths at 2-3 km are attributed to the discontinuity at the interface between the megaregolith and basement, which has been estimated to be in this depth range on Mars, or to the upper limit of non-eruptive dike ascent of magma with a lower volatile content than the shallower dikes. The larger fault-intersection depths (>3 km) within Alba Patera may be due to depression of the megaregolith-basement interface, which may have been depressed due to volcanic construction, burial, and subsidence during the formation of the patera.

4. Within the western hemisphere of Mars there is a dearth of narrow simple grabens with fault-initiation depths less than 0.6- 1.0 km. Application of the Griffith failure criterion to this observation suggests that shear failure is curtailed near the surface of Mars by unfractured rocks with tensile strengths of 2-4 MPa. Failure of near-surface rocks with these tensile strengths results in tension cracks or joints, rather than narrow simple grabens.

ACKNOWLEDGEMENTS

The authors are grateful for the thoughtful and constructive reviews by B. Lucchitta, D. Scott, D. Jankowski, and an anonymous reviewer. Work was supported by grants from the NASA Planetary Geology and Geophysics Program Office to the U.S. Geological Survey and to the Jet Propulsion Laboratory.

REFERENCES

Aggarwal, H. R., and V. R. Oberbeck 1979. Monte Cat 10 simulation of lunar megaregolith and implications. *Proc. Lunar Planet. Sci. Conf. 10th, 2689-2705.*

Baker, V. R., and R. C. Kochel 1979. Martian channel morphology: Maja and Kasei Vanes. *J, Geophys. Res.* 84,7961-7983.

Carr, M. H. 1986. Mars: A water-rich planet? *Icarus* 68, 187-216.

Carr, M. H., and G. G. Schaber 1977. Martian permafrost features. *J. Geophys. Res.* 82, 4039-4054,

Clifford, S. M. 1993. A model for the hydrologic and climatic behavior of water on Mars. *J. Geophys. Res.* 98, 10,973-11,016.

Clifford, S. M., and D. Hillel 1983. The stability of ground ice in the equatorial region of Mars. *J. Geophys. Res.* 88, 2456-2474.

Davis, P. A., and M. P. Golombek 1990, Discontinuities in the shallow Martian crust at Lunae, Syria, and Sinai Plana. *J. Geophys. Res.* 95, 14,231-14,248,

Davis, P. A, and A. S. McEwen 1984. Photoclinometry: Analysis of inherent errors and implications for topographic measurements. *Lunar and Planetary Science XV, 194-195.*

Davis, P. A., and L. A. Soderblom 1984. Modeling crater topography and albedo from monoscopic Viking Orbiter images -- I. Methodology. *J. Geophys. Res.* 89, 9449-9457.

Davis, P. A., and K. L. Tanaka 1993. Small volcanoes in Tempe Terra, Mars: Their detailed morphomet ry and inferred geologic significance (abstract). *Lunar Planet. Sci. Conf.* XXIV, 379-380.

DeHon, R. A. 1985. Ridged plains of Lunae Planum: Thickness distribution revised (abstract). *Lunar Planet. Sci.* XVI, 171-172.

Dreibus, G., and H. Wänke 1985. Mars, a volatile-rich planet. *Meteoritics* **20**, 367-381.

Ernst, R. E., and W. R. A. Baragar 1992. Evidence from magnetic fabric for the flow pattern of magma in the Mackenzie giant radiating dyke swarm. *Nature* 356, 511-513.

Fanale, F. P. 1976. Martian volatiles: Their degassing history and geochemical fate. *Icarus* 28, 179-202.

Fanale, F. P., J. R. Sal vail, A, P. Zent, and S. E. Postawko 1986. Global distribution and migration of subsurface ice on Mars, *Icarus* 67, 1-18.

Farmer, C. B., D. W. Davies, A. L. Holland, D. D. LaPorte, and P. E. Doms 1977. Mars: Water vapor observations from the Viking Orbiters. *J, Geophys. Res.* 82, 4225-4248.

Frey, H. V., and T. D. Grant 1990. Resurfacing history of Tempe Terra and surroundings. *J. Geophys. Res.* 95, 14,249-14,263.

Gatto, L. W., and D. M. Anderson 1975. Alaskan thermokarst terrain and possible Martian analogs. Science **188**, 255-257.

Gibson, I. L., M.N. Sinha, and W.F. Fahrig 1987. The geochemistry of the Mackenzie dyke swarm, Canada. *Geol. Assoc. of Canada Sp. Paper* 34, 109-121.

Golombek, M. P. 1979. Structural analysis of lunar grabens and the shallow crustal structure of the Moon. *J. Geophys. Res.* 84, 4657-4666.

Golombek, M. P. 1985. Fault type predictions from stress distributions on planetary surfaces: Importance of fault initiation depth. *J. Geophys. Res.* 90, 3065-3074.

Golombek, M. P., and G. E. McGill 1983. Grabens, basin tectonics, and maximum total expansion of the moon. *J. Geophys. Res.* 88, 3563-3578.

Greeley, R. 1987. Release of juvenile water on Mars: Estimated amounts and timing associated with volcanism. *Science 236,* 1653-1654.

Haimson, B. C., and F. Rummel 1982. Hydrofracturing stress measurements in the Iceland research drilling project drill hole at Reydarfjordur, Iceland. *J. Geophys. Res.* 87, 6631-6649.

Hartmann, W. K. 1980. Dropping stones in magma oceans: Effects of early lunar cratering. In *Proceedings of the Conference on Lunar Highlands Crust. (.I,* J. Papike and R. B. Merrill, Eds.), pp. 155-171. Pergamon, New York.

Hörz, F., R, V. Gibbons, R. E. Hill, and D. E. Gault 1976. Large scale cratering of the lunar highlands: Some Monte Carlo model considerations. *Proc. Lunar Sci. Conf. 7th,* 2931-2945,

Jankowski, D. G. and S. W. Squyres 1991. Sources of error in planetary photoclinometry. *J. Geophys. Res.* 96, 20,907-20,922.

Jankowski, D. G., and S. W. Squyres 1992. The topography of impact craters in "softened" terrain on Mars. *Icarus 100,* 26-39.

Kochel, R. C., and C. M. Burgess 1982. Structural cent rol of geomorphic features in the Kasei Vanes region of Mars. *NASA Tech. Memo. 85127, 288-290.*

Kokelaar, B.P. 1982. Fluidization of wet sediments during the emplacement and cooling of various igneous bodies. *J. Geol. Sot. London,* **139,** *21-33.*

Lister, J. R. 1990. Buoyancy-driven fluid fracture: the effects of material toughness and of low viscosity precursors. *J. Fluid. Mech.* 210, 263-280.

Lister, J. R. 1991. Steady solutions for feeder dikes in a density-stratified lithosphere. *Earth Planet, Sci. Lttrs. 107, 233-242.*

Lucchitta, B. K., R. A. Balzer, and L. M. Bertolini 1990. Vanes Marineris, Mars: Are pit chains formed by erosion and troughs by tectoni sm? (abstract). *Lunar Planet. Sci. XXI, 722-723.*

MacKinnon, D. J., and K. L.. Tanaka 1989. The impacted Martian crust: Structure, hydrology, and some geologic implications. *J. Geophys. Res.* 94, 17,359-17,370.

Mastin, L. G., and D. D. Pollard 1988. Surface deformation and shallow dike intrusion processes at Inyo Craters, Long Valley, California. *J. Geophys. Res.* 93, 13,221-13,235.

McGill, G, E., and A. W. Stromquist 1979. The grabens of Canyonlands National Park, Utah: Geometry, mechanics, kinematics. *J. Geophys. Res.* 84, 4547-4563.

McKenzie, D., J. M, McKenzie, and R. S. Saunders 1992. Dike emplacement on Venus and Earth. *J. Geophys. Res.* 97, 15,977-15,990.

Mellon, M. T., and B. M. Jakosky 1993. Geographic variations in the thermal and diffusive stability of ground ice on Mars. *J. Geophys. Res.* 98, 3345-3364.

Melosh, H. J., and C. A. Williams 1989. Mechanics of graben formation in crustal rocks: A finite element analysis. *J. Geophys. Res.* 94, 13,961-13,973.

Minnaert, M. 1941. The reciprocity y principle in lunar photometry. *Astrophys. J.* 93, 403-410.

Moore, H. J., and C. A. Hodges 1980. Some Martian volcanic centers with small edifices. *NASA Tech. Memo. 82385, 266-268.*

Mouginis-Mark, P. J., L. Wilson, and J.R. Zimbelman 1988. Polygenic eruptions on Alba Patera, Mars. *Bull. Volcanol.* 50, 361-379.

Opheim, J. A., and A. Gudmundsson 1989. Formation and geometry of fractures, and related volcanism, of the Krafla fissure swarm, northeast Iceland. *Geol.* Sot. *Amer. Bull.* **101,** 1608-1622.

Paige, D. A. 1992. The thermal stability of near-surface ground ice on Mars. *Nature* 356, 43-45,

Parfitt, E. A. 1991. The role of rift zone storage in cent rolling the site and timing of eruptions and intrusions of Kilauea volcano, Hawaii. *J. Geophys. Res. 96, 10,101-10,112.*

Parfitt, E. A., and J. W. Head 1993. Buffered and unbuffered dike emplacement on Earth and Venus: Implications for magma reservoir size, depth, and rate of magma replenishment. *Earth,* Moon *and Planets* **61,** 249-281.

Pike, R. J., and P. A. Davis 1984. Toward a topographic model of Martian craters from photoclinometry (abstract). *Lunar Planet. Sci.* XV, *645-646.*

Plescia, J. B, 1981. The Tempe volcanic province of Mars and comparisons with the Snake River Plains of Idaho. *Icarus 45, 586-601.*

Plescia, J. B. 1991, Graben and extension in northern Tharsis, Mars. *J. Geophys. Res.* 96, 1 8,883-18,895.

Pollard, D. D. 1976. On the form of open hydraulic fractures in the Earth's crust. *Geophys. Res. Lttrs. 3, 513-516.*

Rossbacher, L. A., and S. Judson 1981. Ground ice on Mars: inventory, distribution, and resulting landforms. *Icarus* 45,39-59.

Rubin, A. M, 1992. Dike-induced faulting and graben subsidence in volcanic rift zones. *J. Geophys. Res. 97,* 1839-1858.

Rubin, A. M., and D. D. Pollard 1988. Dike-induced faulting in rift zones of Iceland and Afar. Geology 16,413-417.

Ryan, M. P. 1987. Elasticity and contractancy of Hawaiian olivine tholeiite and its role in the stability and structural evolution of subcaldera magma reservoirs and rift systems. In *Volcanism in Hawaii, U.S. Geol. Surv. Prof. Paper 1350,* Chap. 52, (R. W. Decker, T. L. Wright, and P. H. Stauffer, Eds.), pp. 1395-1447.

Schneeberger, D. M., and D. C. Pieri, 1991. Geomorphology and stratigraphy of Alba Patera, Mars, *J. Geophys. Res. 96, 1907-1930.*

Schultz, R. A. 1989. Do pit-crater chains grow up to be. Vanes Marineris canyons? In *MEVTV Workshop on Tectonic Features on Mars, Tech. Rep. 89-06,* (T. R. Walters and M. P. Golombek, Eds.), pp. 47-48. Lunar and Planetary Institute, Houston.

Schultz, R. A. 1993. Brittle strength of basaltic rock masses with applications to Venus: *J. Geophys. Res. 98, 10,883-10,895.*

Schumm, S. A. 1974. Structural origin of large Martian channels. *Icarus 22, 371-384.*

Scott, D. H., and J. M. Dohm 1990. Faults and ridges: Historical development in Tempe Terra and Ulysses Patera region of Mars. *Proc. Lunar and Planet. Sci. Conf. 20th, 503-513.*

Scott, D. H., and K. L. Tanaka 1986. Geologic map of the western equatorial region of Mars, scale 1:15,000,000. *U.S. Geol. Sum. Misc. Invest. Ser. Map 1-1802-A.*

Sharp, R. P. 1973a. Mars: Troughed terrain. *J. Geophys. Res.* 78, 4063-4072.

Sharp, R. P. 1973b. Mars: Fretted and chaotic terrains. *J. Geophys. Res. 78, 4073-4083.*

Short, N. M., and M. L. Forman 1972. Thickness of impact crater ejecta on the lunar surface. *Mod. Geol.* **3**, *69-91.*

Smoluchowski, R. 1968. Mats: Retention of ice. *Science 159, 1348-1350.*

Soderblom, L. A., and D. B, Wenner 1978. Possible fossil H_20 liquid-ice interfaces in the Martian crust. *Icarus* 34, 622-637.

Squyres, S. W., and M, H. Carr 1986. Geomorphic evidence for the distribution of ground ice on Mars. *Science 231, 249-252.*

Tanaka, K. L. 1990, Tectonic history of the Alba Patera-Ceraunius Fossae region of Mars. *Proc. Lunar and Planet. Sci. Conf. 20th, 515-523.*

Tanaka, K. L., and M. G. Chapman 1992. Kasei Vanes, Mars: Interpretation of canyon materials and flood sources. *Proc. Lunar and Planet. Sci. Conf. 22nd, 73-83.*

Tanaka, K. L., and P. A. Davis 1988. Tectonic history of the Syria Planum province of Mars, *J. Geophys. Res. 93, 14,893-14,917.*

Tanaka, K. L., and M. P. Golombek 1989. Martian tension fractures and the formation of grabens and collapse features in Vanes Marineris. *Proc. Lunar and Planet. Sci. Conf. 19th, 383-396.*

Tanaka, K. L., M, P. Golombek, and W. B. Banerdt 1991. Reconciliation of stress and structural histories of the Tharsis region of Mars. *J. Geophys. Res.* 96, 15,617-15,633.

Thorpe, T. E. 1973. Mariner 9 photometric observations of Mars from November 1971 through March 1972. *Icarus* 20, 482-489.

U.S. Geological Survey 1982a, Shaded-relief map of Mare Acadalium Quadrangle of Mars, scale 1:5,000,000, *U.S. Geol. Surv. Topog. Ser. I-1476.*

U.S. Geological Survey 1982b. Shaded-relief map of Mare Arcadia Quadrangle of Mars, scale 1:5,000,000; *U.S. Geol. Surv. Topog. Ser. I-1477.*

U.S. Geological Survey 1985. Shaded-relief map of Mars, western region, scale 1:15,000,000, *U.S. Geol. Surv. Misc. Invest. Ser. I-1618,* sheet 2.

U.S. Geological Survey 1989. Topographic map of the western equatorial region of Mars, scale 1:15,000,000, U.S. *Geol. Surv. Misc. Invest. Ser. 1-2030,* sheet 2.

Walker, J. C. G. 1977. *Evolution of the Atmosphere.* McMillan, New York, 318 pp.

Wilson, L., and J. W. Head 1981. Ascent and eruption of basaltic magma on the Earth and Moon. *J. Geophys. Res.* 86, 2971-3001.

Wilson, L., and J. W. Head 1994. Mars: Review and analysis of volcanic eruption theory and relationships to observed landforms. *Reviews of Geophysics 32, 221-263.*

Wise, D. U. 1979. Geologic map of the Arcadia quadrangle of Mars, scale 1:5,000,000. *U. S. Geol. Surv. Misc. Invest. Ser. Map, I-1154.*

Witbeck, N. E., and J. R. Underwood 1984. Geologic map of Mare Acidalium quadrangle, Mars, scale 1:5,000,000. *U. S. Geol. Surv. Misc. Invest. Ser. Map, 1-1614.*

Woronow, A. 1988. Variation in the thickness of ejects cover on Mars with increasing crater density. In *MEVTV Workshop on Nature and Composition of Surface Units on Mars, Tech. Rep. 88-05* (J. R. Zimbelman, S. C. SoIonIon, and V. 1... Sharpton, Eds.), pp. 135-137. Lunar and Planetary Institute, Houston,

Table 1. Morphometric Characteristics of Erosional Landforms in the Tempe Terra Region of Mars.

Features	Number of Features Measured[1]	Scarp Height (m ± 1σ)	Scarp Slope (deg ± 1σ)	Rim-to-rim width (km ± 1σ)
Irregular Depressions	10	107 ± 44	6.6 ± 1.3	3.8 ± 2.0
Fretted Fractures	32	505 ± 255	19.0 ± 3.8	3.3 ± 2.4
Troughs and Pits	49	374 ± "357	21.3 ± 4.1	4.2 ± 3.2
Solitary Scarps	124	658 ± 478	24.9 ± 9.9	n.a.[2]

[1] Multiple profiles were obtained for the larger features that appeared to have variable morphometries; their average morphometries were used in tabulation of average landform morphometries.

[2] n.a. = not applicable

able II. Means and Standard Deviations for Topographic Characteristics of Simple Grabens within Tempe Terra and Alba Patera regions.

ultSet/Stage and Age	Fault Trend	Number Measured	Wall Depth (m ± 1σ)	Wall Slope (deg ± 1σ)	Rim-to-rim Width (km ± 1σ)	Fault-intersection Depth[1] (km ± 1σ)
MPE TERRA REGION:[2]						
Noachian System						
Set 1 - Lower-Middle Noachian	N	3	81 ± 46	8.4 ± 3.1	2.7 ± 0.5	1.8 ± 0.3
Set 2 - Middle Noachian	Nw	1	59	4.9	3.9	2.8
Set 3 - Middle Noachian	NE	43	78 ± 45	8.5 ± 3.4	2.4 ± 1.1	1.6 ± ().8
Set 4 - Middle Noachian	N	20	62 ± 29	10.6 ± 3.9	1.4 ± 0.7	0.9 ± 0.5
Set 5 - Middle-Upper Noachian	NE	37	131 ± 110	11.6 ± 4.6	2.5 ± 0.9	1.6 ± ().7
Hesperian System						
Set 1 - Lower Hesperian	NE	17	67 ± 39	9.8 ± 4.0	1.7 ± 0.7	1.1 ± 0.5
Set 2 - Upper Hesperian	NE	66	84 ± 66	8.3 ± 3.8	2.4 ± 1.2	1.5 ± 0.9
Set 3 - Upper Hesperian-Middle Amazonian	NE/NW	11	82 ± 20	8.7 ± 2.8	2.2 ± 0.4	1.5 ± 0.3
Average of 198 Grabens:			87 ± 71	9.4 ± 4.1	2.2 ± 1.1	1.4 ± 1.2

ble II (con't)

ult Set/Stage and Age	Fault Trend	Number Measured	Wall Depth (m ± 1σ)	Wall Slope (deg ± 1σ)	Rim-to-rim Width (km ± 1σ)	Fault-intersection Depth[1] (km ± 1σ)
BA PATERA REGION:[3]						
Stage I - Noachian	NE	2	33 ± 11	4.4 ± 0.8	2.9 ± 1.4	2.1 ± 1.2
Stage II - Late Noachian-Hesperian	N	2	75 ± 17	9.7 ± 2.4	1.7 ± 0.2	1.0 ± 0.2
Stage III - Early Amazonian	N	105	97 ± 82	9.2 ± 4.4	3.8 ± 1.8	2.8 ± 1.4
Stage 111/IV - Early-Late Amazonian	N	20	49 ± 23	6.2 ± 2.8	2.8 ± 0.9	2.0 ± 0.8
Stage IV - Middle-Late Amazonian	N	43	43 ± 25	5.2 ± 3.0	2.6 ± 1.2	1.8 ± 1.0
Average of 172 grabens:			77 ± 70	7.8 ± 4.3	3.4 ± 1.7	2.8 ± 1.7

alculated from topographic data using method of Golombek 1979 and assuming 60° fault dips.

s defined by Scott and Dohm 1990.

s defined by Tanaka 1990.

Table III. Comparison of Average Scarp Heights and Average Fault-intersection Depths within Geologic Units Exposed in the Tempe Terra Region of Mars.

Geologic Unit [1]	Number of Features Measured[2]: Scarps	Number of Features Measured[2]: Grabens	Scarp Height (km ± 1σ)	Fault-Intersection Depth[3] (km ± 1σ)
Hcht	3		0.9 ± 0.2	n.d.[4]
Htu	9	17	0.2 ± 0.05	1.6 ± ().9
Htm	2	12	1.5 ± 0.01	1.3 ± 0.5
Ht 1	25	2	0.6 ± 0.5	0.6 ± 0.1
Hr	62	27	0.6 ± 0.4	1.1 ± 0.4
Nple	10		0.1 ± 0.04	n.d.
Npl1	31	28	0.5 ± 0.6	1.6 ± 0.8
Nplh	34	13	0.4 ± 0.3	1.3 ± 0.2
Nf	33	88	0.4 ± 0.2	1.4 ± 0.8
Nb	13		1.1 ± 0.4	n.d.

[1] As defined by Scott and Tanaka 1986.

[2] Multiple profiles were obtained on features that appeared to have variable morphometries; their average morphometries were used in the tabulation of average scarp height and fault-intersection depth.

[3] Calculated from topographic data using method of Golombek 1979 and assuming 60° fault dips.

[4] n.d. = no data within this unit.

FIGURE CAPTIONS

Figure 1, Shaded-relief map of part of western Mars (U.S. Geological Survey 1985) showing the locations of the Tempe Terra and Alba Patera study areas.

Figure 2. Geologic map of the Tempe Terra region (based on the map of Scott and Tanaka 1986) showing locations (closed circles) of photoclinometric measurements of troughs and pits, fretted fractures, irregular depressions, and solitary scarps. Units include the basement complex (Nb), fractured material (Nf), hilly unit (Nplh), cratered unit (Npl_1), and etched unit (Nple) of Noachian age; the ridged plains (Hr), Tempe Terra Formation (Htl, Htm, Htu), chaotic terrain (Hcht), and lower member of the Alba Patera formation (Hal) of Hesperian age; volcanoes (V) of Hesperian and Noachian age; and the Arcadia formation (Aa_1) of Amazonian age.

Figure 3. Geologic map of the eastern Alba Patera region (generalized from Scott and Tanaka 1986 and Mouginis-Mark *et al. 1988)* showing calculated fault-intersection depths (rounded to nearest km) at locations of graben measurements. Units include the fractured material (Nf) and cratered unit (Npl_1) of Noachian age; the Ceraunius Fossae formation (AHcf) and dissected unit (Had) of Hesperian age; and the Alba Pat era formation (Hal, A am, Aau) of Hesperian and Amazonian age.

Figure 4. Irregular depressions in the Noachian etched unit (Nple) in eastern Tempe Terra, Mars (Viking Orbiter frame 258 S23). Frame center at 43.9° N lat., 55.9° ion. (Fig. 2). Lines indicate profiles and numbers indicate depths (km) of photoclinometric measurements.

Figure 5, Flat-floored troughs and pits in the lower member of the Tempe Terra Formation (Htl) in western Tempe Terra, Mars (Viking Orbiter 1 image mosaic of rev. 627). Mosaic center at 39.10 N lat., 86.1” Ion. (Fig. 2). Lines indicate profiles and numbers indicate depths/heights (km) of photoclinometric measurements. Scarp profiles of north-trending troughs of Mareotis Fossae indicated by letters A, B, and C. Trough D extends for about 70 km; its depth increases from about 0.4 km in the northeast to the depth of the Tempe Terra border scarps. Examples of a pit, pit chain, trough, and simple graben are indicated.

Figure 6. Fretted fractures in Hesperian ridged plains unit (Hr) in southern Tempe Terra, Mars (Viking Orbiter frame 555 A12). Frame center at 30.7° N lat., 72.4° W ion. (Fig. 2). Lines indicate profiles and numbers indicate depths (km) of photoclinometric measurements.

Figure 7, Solitary scarps bounded by planar surfaces in the Hesperian ridged plains unit (Hr) along the southeastern margin of Tempe Terra, Mars (Viking Orbiter frame 668A1 6). Frame center at 32.6° N lat., 54.2° ion. (Fig, 2). Lines indicate profiles and numbers indicate heights (km) of photoclinometric measurements.

Figure 8. Index map of Tempe Terra region (based on U.S. Geological Survey 1982a,b) showing simple grabens (solid lines) and locations of photoclinometric profiles (closed circles).

Figure 9. Index map of Alba Patera region (based on U.S. Geological Survey 1982b) showing simple grabens (solid lines) and locations of photoclinometric profiles (closed circles).

Figure 10. Frequency histograms of measured populations of irregular depression depths, fretted fracture depths, trough and pit depths, and solitary scarp heights in the Tempe Terra region.

Figure 11. Frequency histograms of measured populations of all measured erosional scarp heights/depths within different geologic units in the Tempe Terra region,

Figure 12. Frequency histogram of percentage of measured population of calculated fault-intersection depths in the Tempe Terra and Alba Patera regions.

Figure 13. Frequency histograms of estimated fault-intersection depths within different geologic units in the Tempe Terra region.

Figure 14. Elevations of intersections of faults bounding simple grabens in the Alba Patera region, The closed circle was obtained for a simple graben in Noachian Tempe Terra plateau material.

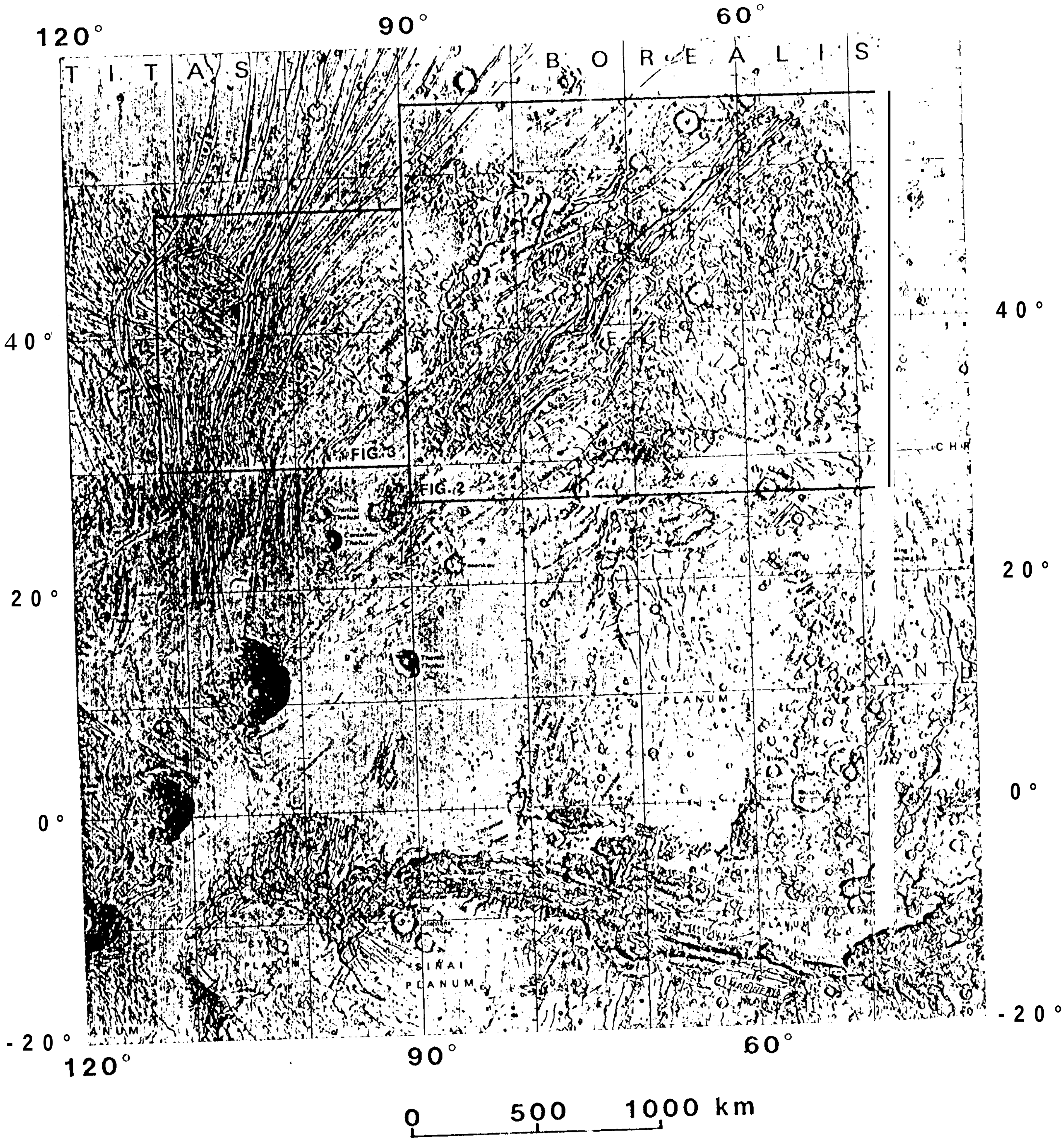
120°
90°
60°
T I T A S
B O R E A L I S
40°
20°
0°
-20°
FIG. 3
FIG. 2
LUNAE
PLANUM
SINAI
PLANUM
0 500 1000 km

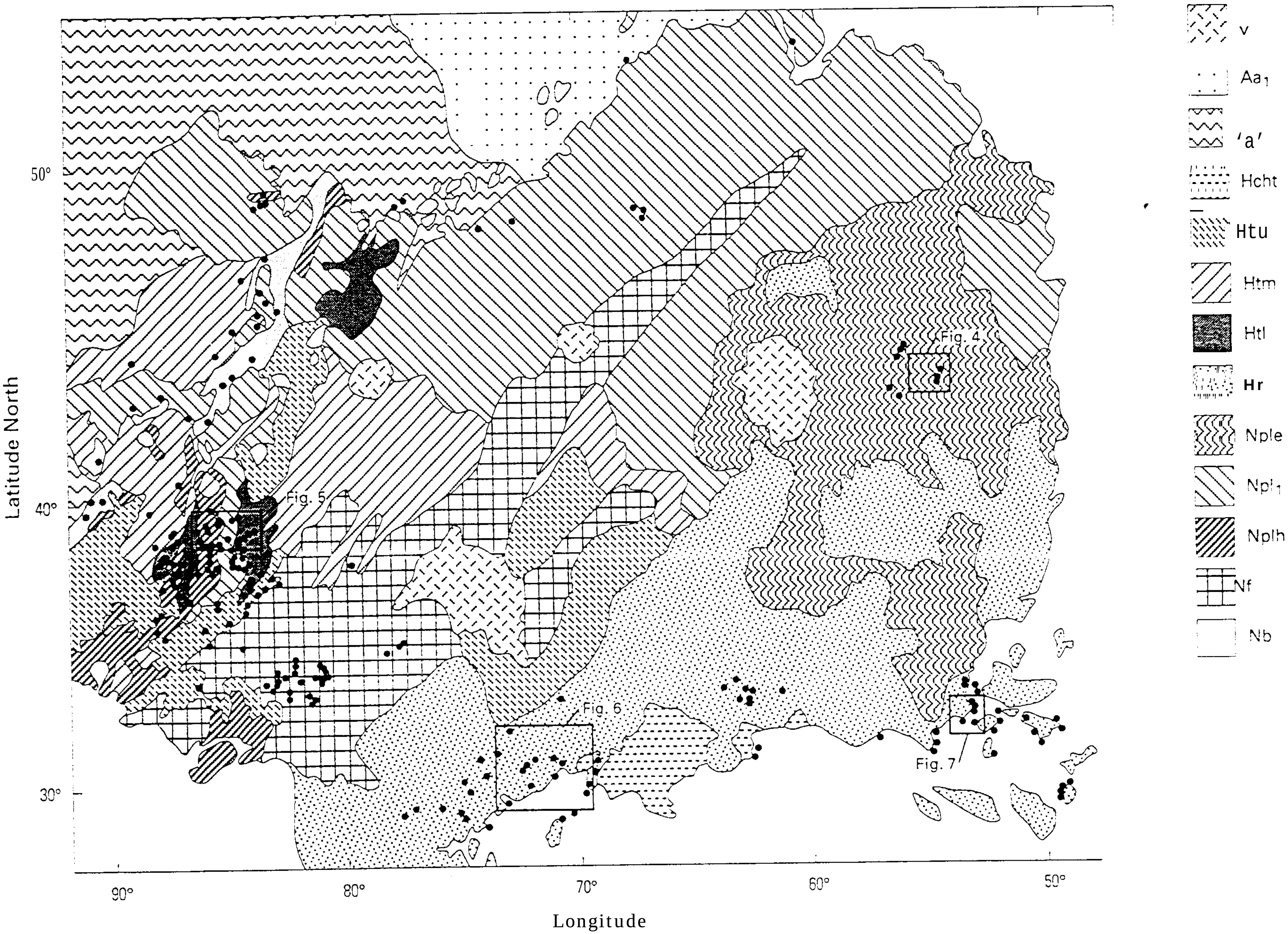

v
Aa1
'a'
Hcht
Htu
Htm
Htl
Hr
Nple
Npl1
Nplh
Nf
Nb
Fig. 4
Fig. 5
Fig. 6
Fig. 7
50°
40°
30°
90°
80°
70°
60°
50°
Latitude North
Longitude

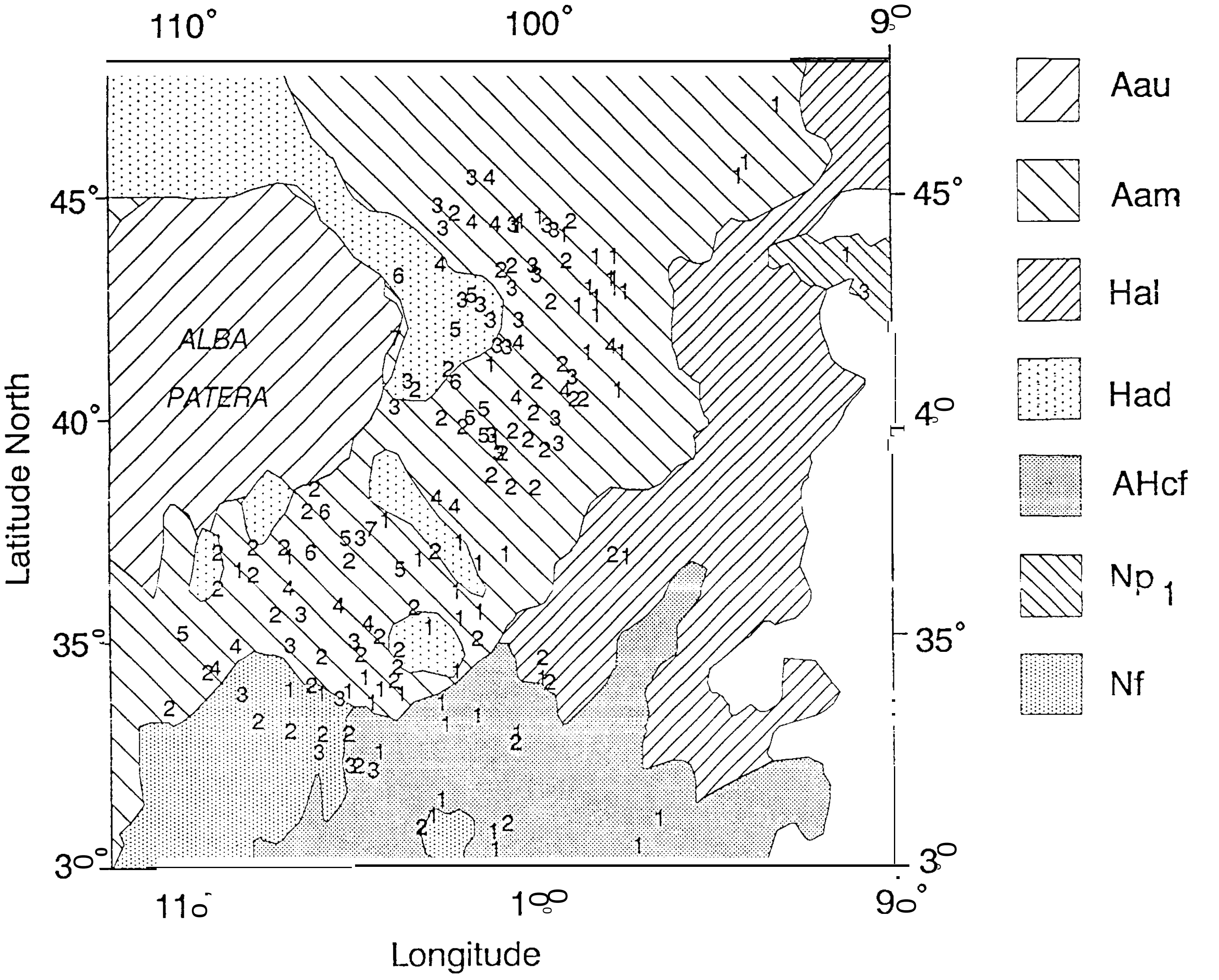

110°
100°
90°
45°
40°
35°
30°
Latitude North
Longitude
ALBA
PATERA
Aau
Aam
Hal
Had
AHcf
Np 1
Nf

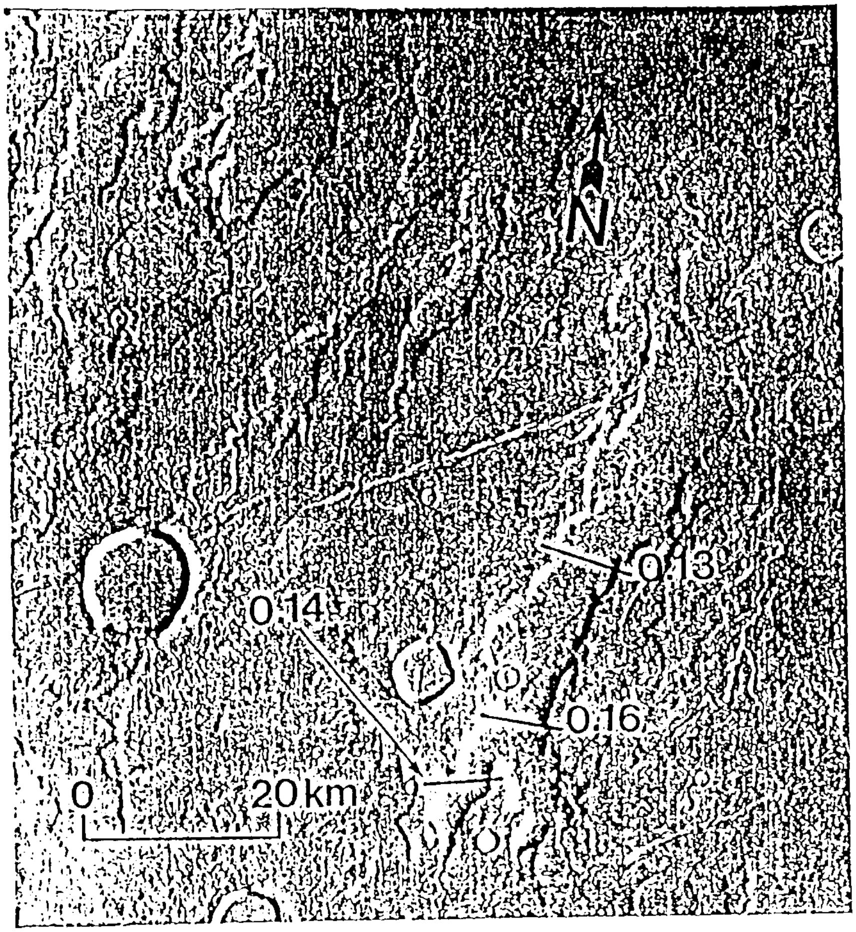

FIG. 4

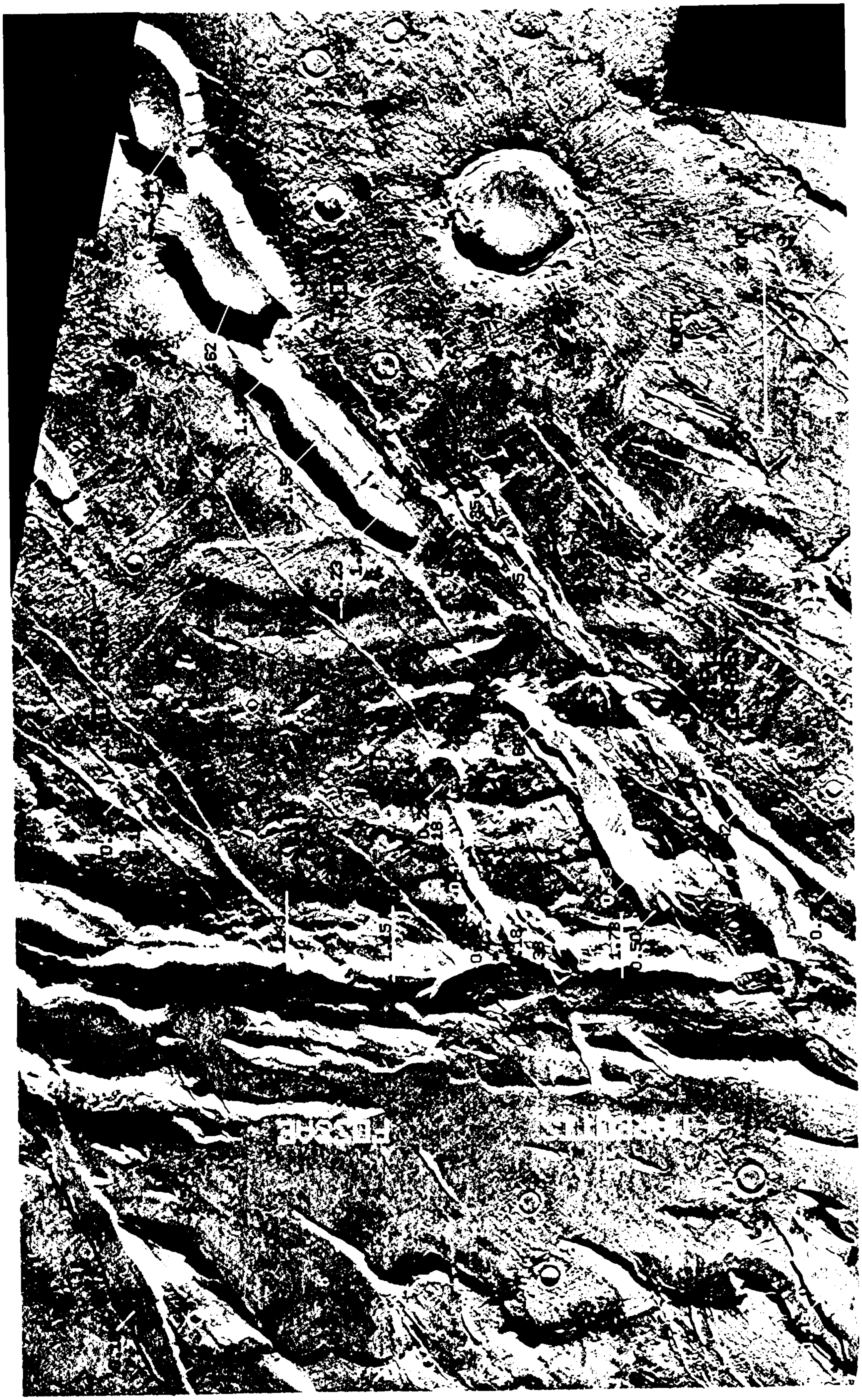

FIG. 5

FIG. 6

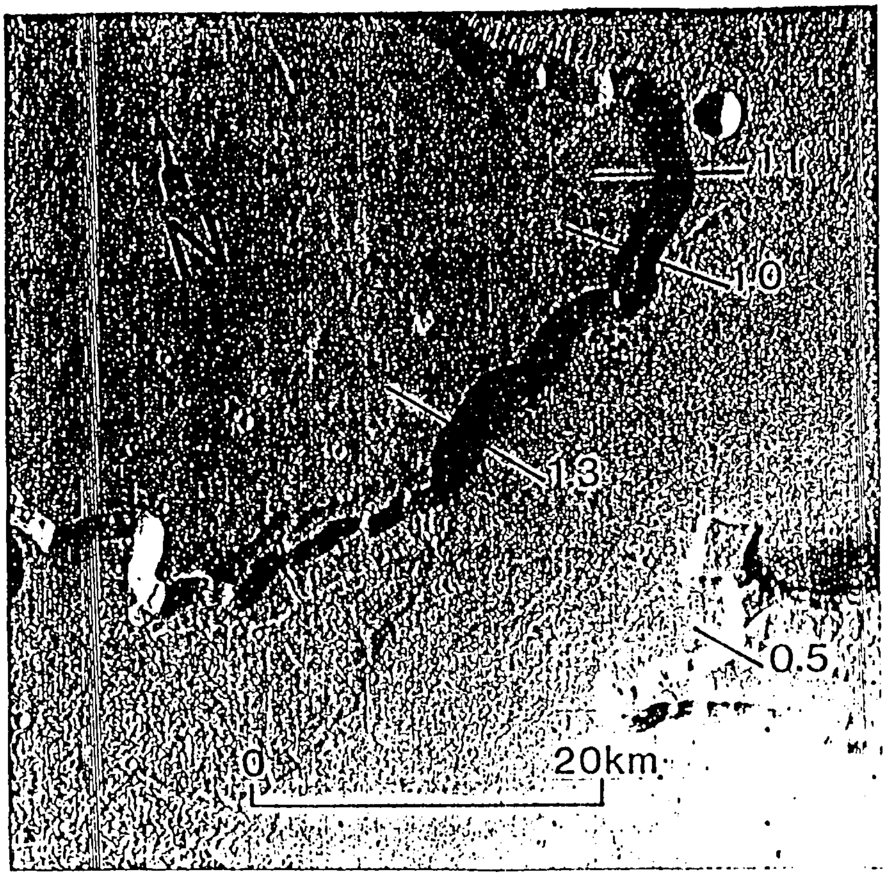

FIG. 7

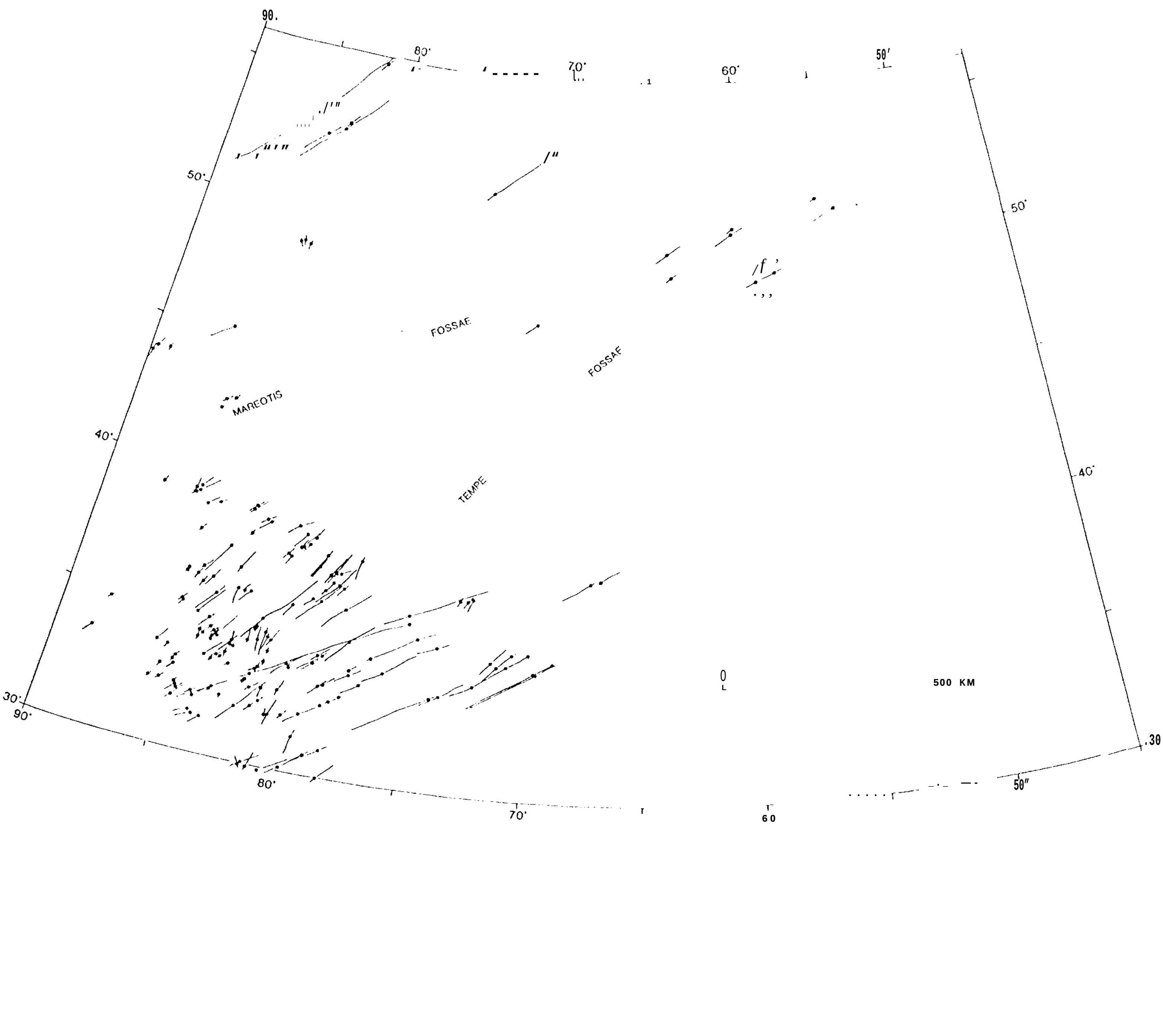

90.
80°
70°
60°
50′
50°
40°
30°
90°
80°
70°
60
50″
.30
50°
40°
FOSSAE
FOSSAE
MAREOTIS
TEMPE
0
500 KM

FIG. 8

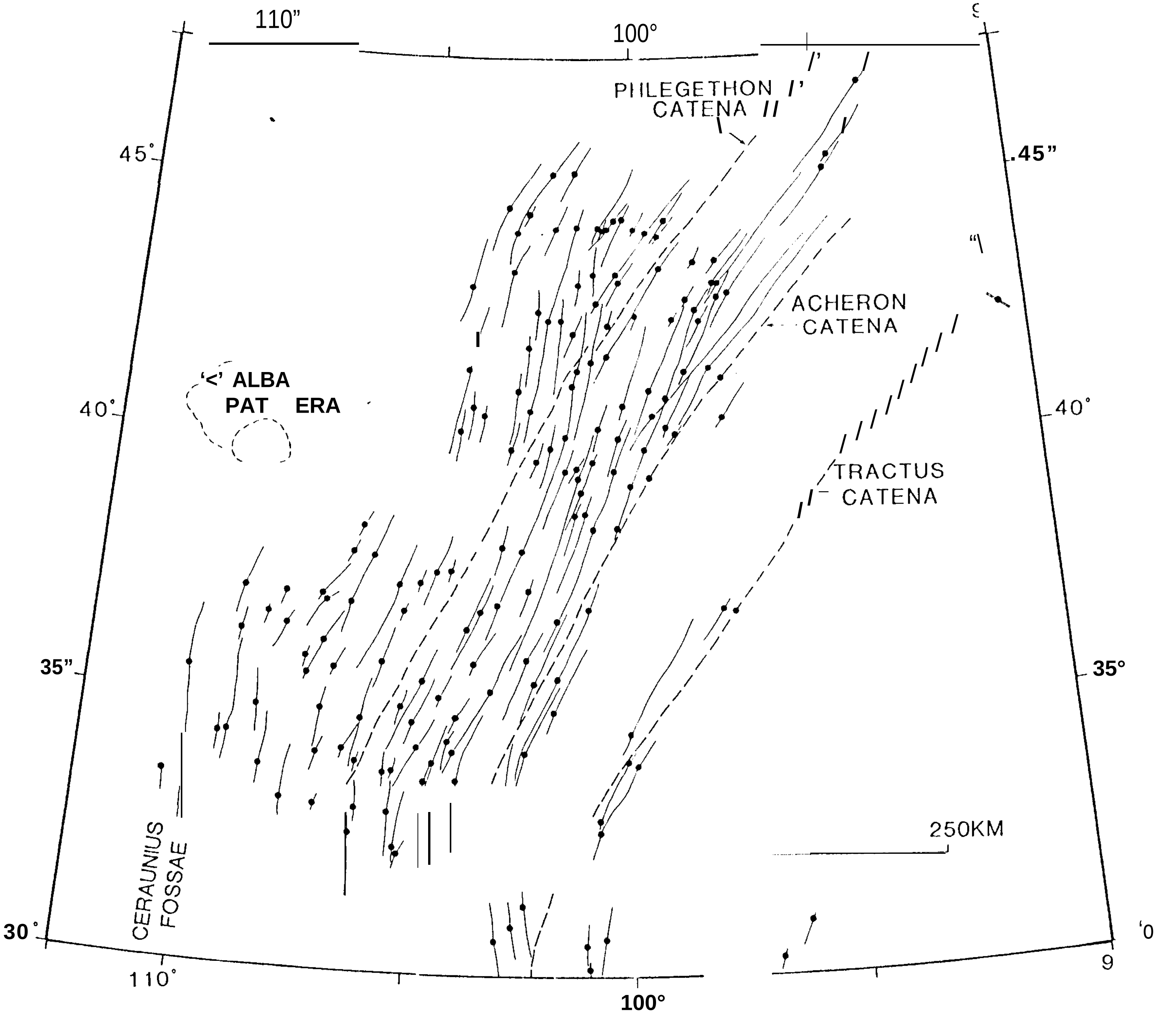

110"
100°
PHLEGETHON
CATENA
45°
.45"
ACHERON
CATENA
ALBA
PAT ERA
40°
40°
TRACTUS
CATENA
35"
35°
250KM
CERAUNIUS
FOSSAE
30°
110°
100°

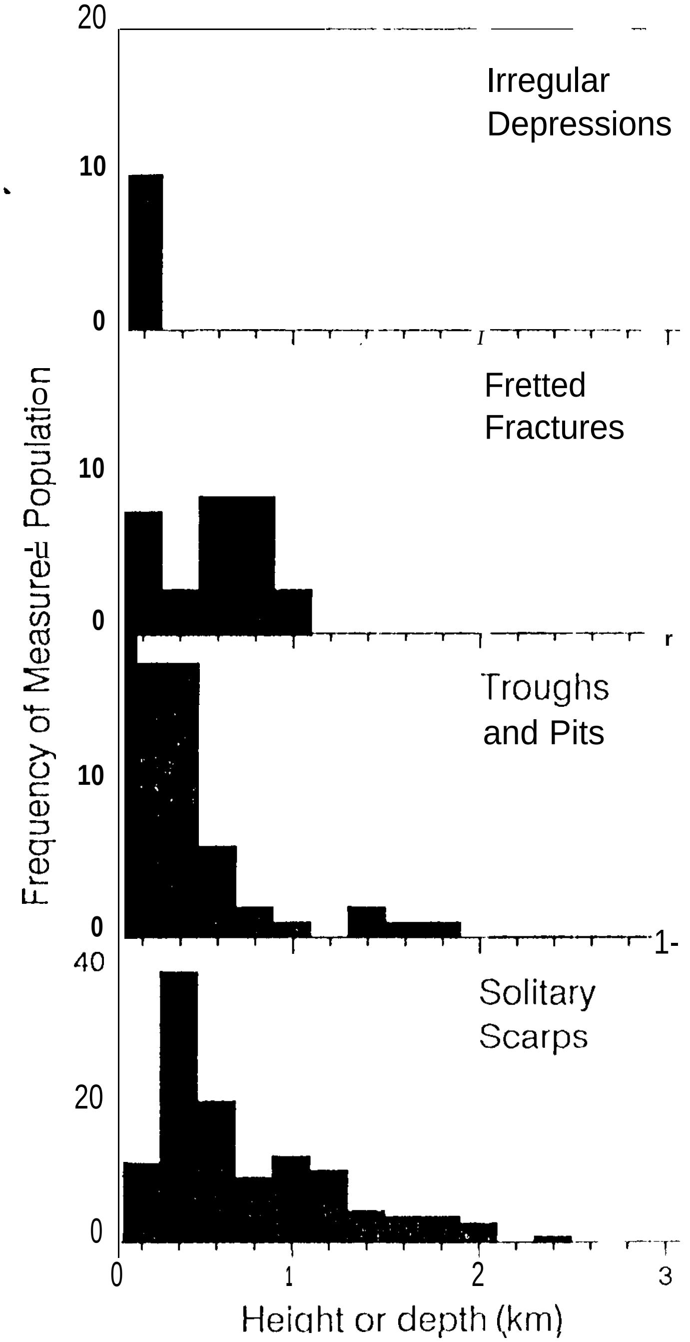
Irregular
Depressions
Fretted
Fractures
Troughs
and Pits
Solitary
Scarps
Frequency of Measured Population
Height or depth (km)
20
10
0
10
0
10
0
40
20
0
0
1
2
3

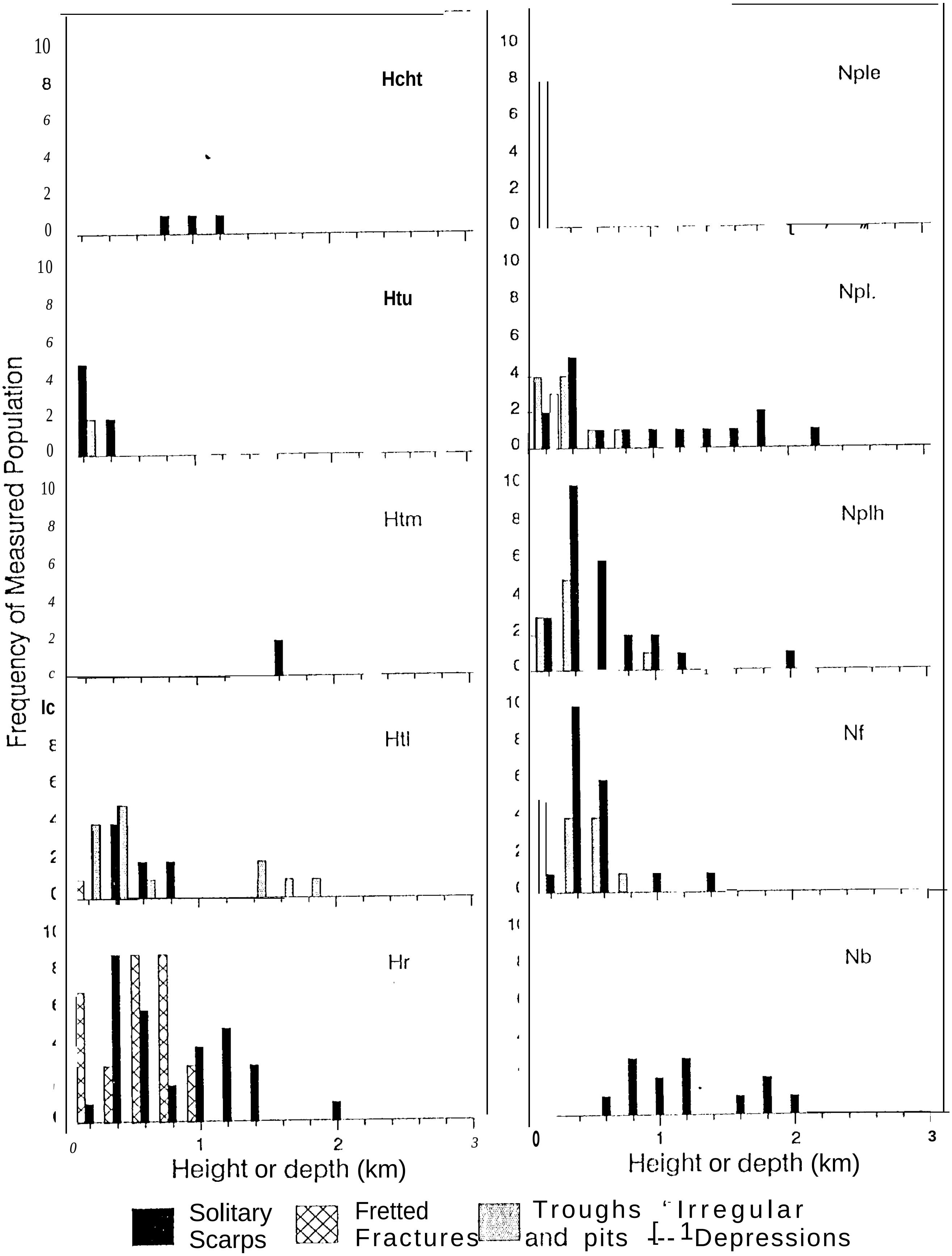
Frequency of Measured Population
Hcht
Htu
Htm
Htl
Hr
Nple
Npl.
Nplh
Nf
Nb
Height or depth (km)
Height or depth (km)
Solitary Scarps
Fretted Fractures
Troughs and pits
Irregular Depressions

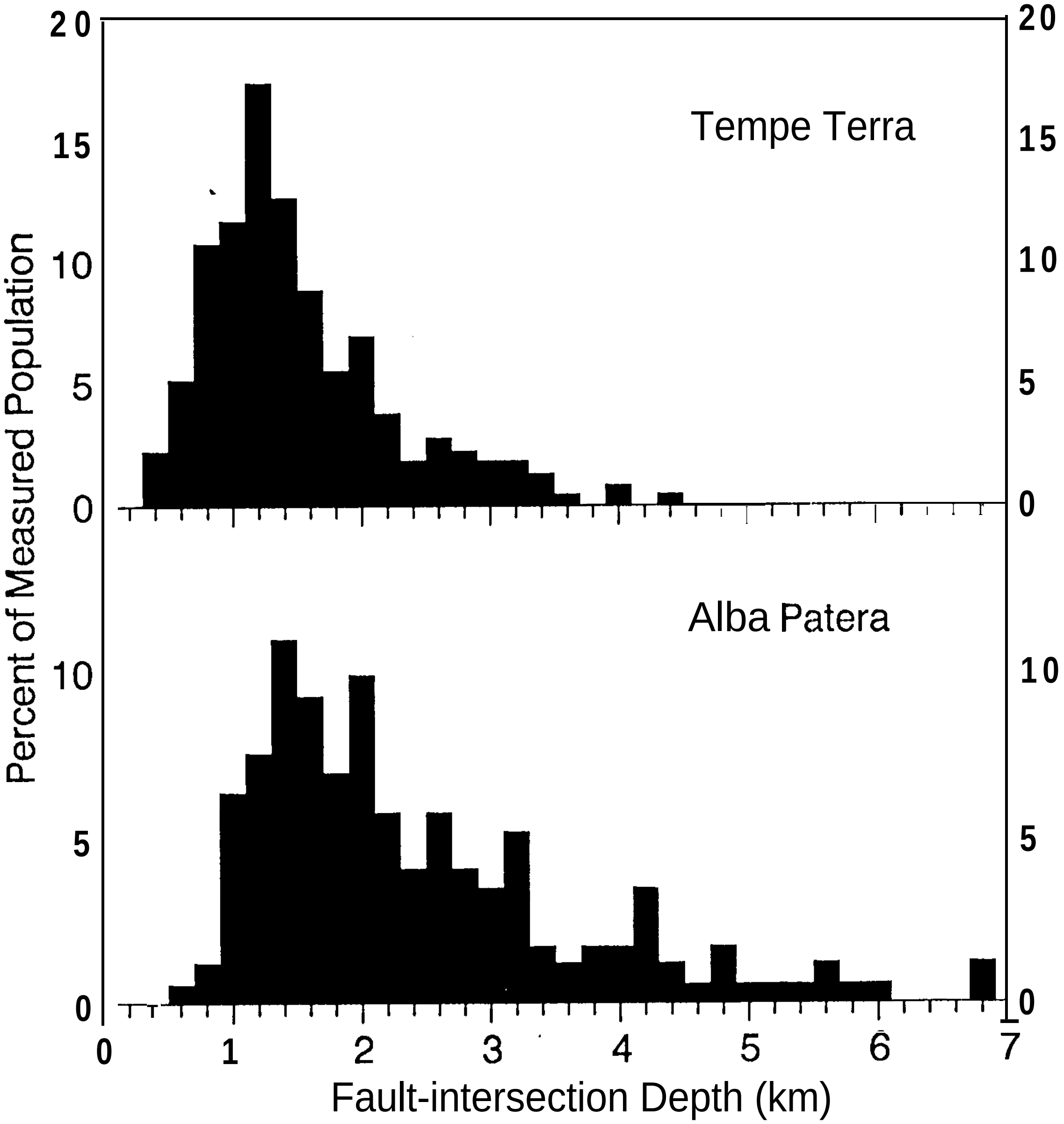

Tempe Terra
Alba Patera
Percent of Measured Population
Fault-intersection Depth (km)
0
1
2
3
4
5
6
7
0
5
10
15
20

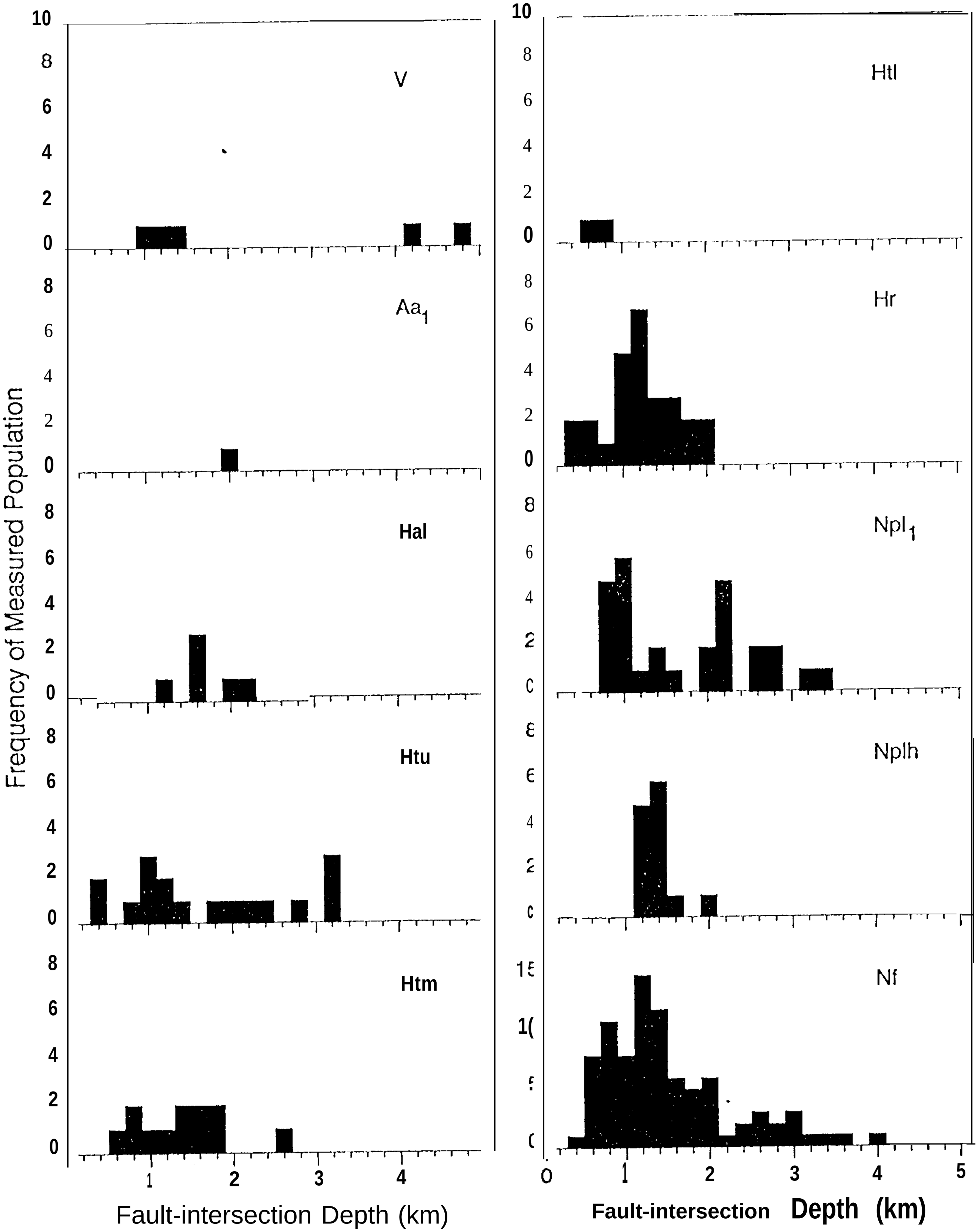

Frequency of Measured Population
V
Aa1
Hal
Htu
Htm
Htl
Hr
Npl1
Nplh
Nf
Fault-intersection Depth (km)
Fault-intersection Depth (km)

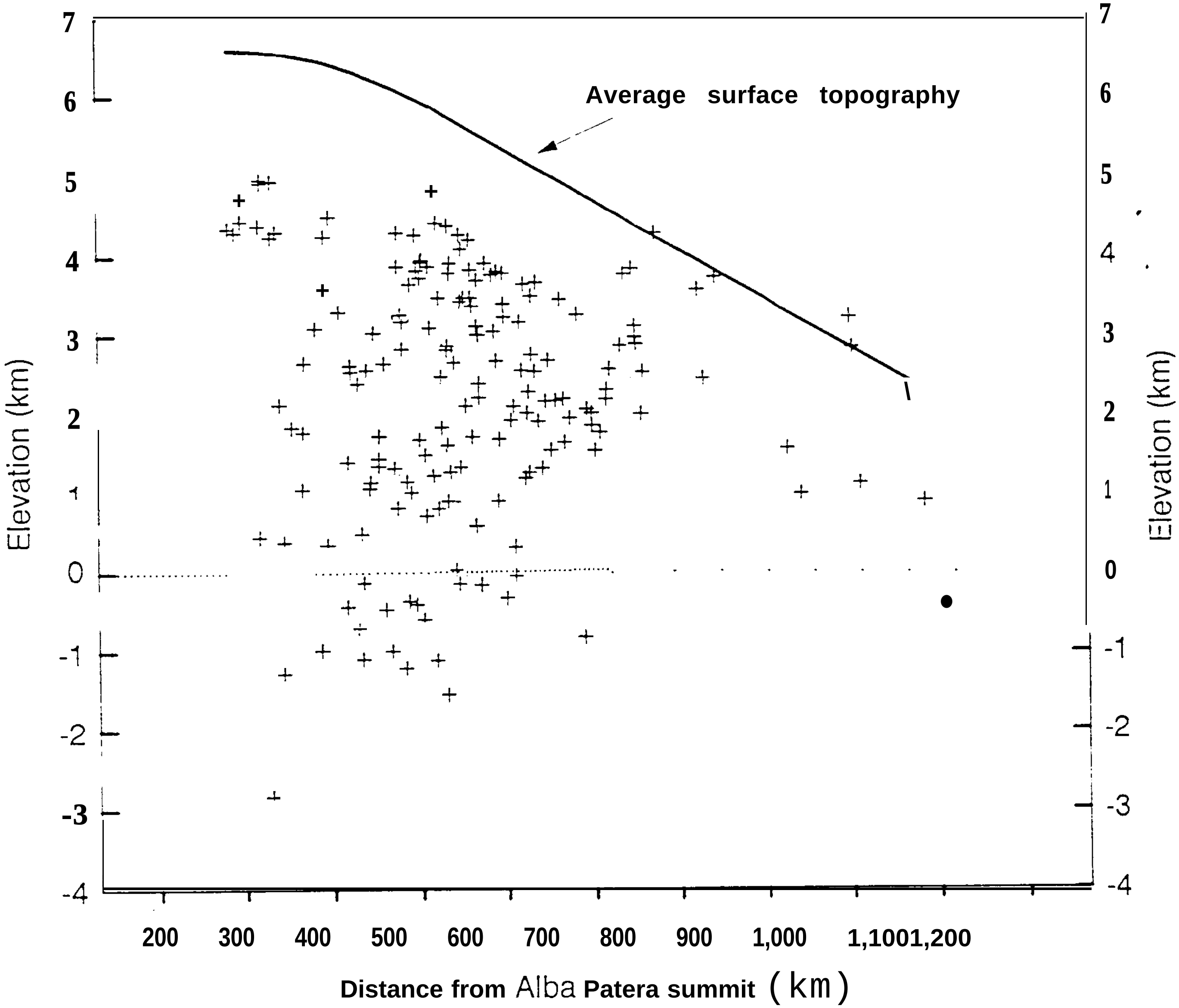

Average surface topography
Elevation (km)
7
6
5
4
3
2
1
0
-1
-2
-3
-4
200
300
400
500
600
700
800
900
1,000
1,100
1,200
Distance from Alba Patera summit (km)